**Title**
Systems Genomics to Dissect the Metabolic Components of Alzheimer’s Disease



**Author**
Ding, Jessica Aliyah

**Publication Date**
2020

Peer reviewed|Thesis/dissertation

UNIVERSITY OF CALIFORNIA

Los Angeles

# Systems Genomics to Dissect the Metabolic Components of Alzheimer's Disease

A thesis submitted in partial satisfaction

of the requirements for the degree Master of Science

in Physiological Science

by

Jessica Aliyah Ding

2020

ABSTRACT OF THE THESIS

Systems Genomics to Dissect the
Metabolic Components of Alzheimer's Disease

by

Jessica Aliyah Ding

Master of Science in Physiological Science
University of California, Los Angeles, 2020
Professor Xia Yang, Chair

Alzheimer's disease (AD) is a chronic neurodegenerative disease that accounts for most cases of dementia. Progressive neuronal atrophy and the decline of cognitive function observed in AD results from the accumulation of extracellular amyloid-β (Aβ) and intraneuronal aggregates of hyperphosphorylated tau. Emerging evidence supports the importance of metabolic dysregulation in AD, but the underlying mechanisms and connections between metabolism and Aβ accumulation remain elusive. We conducted a two-part study to dissect the metabolic components of AD. In a human study, we investigated the shared genetically perturbed pathways between AD and type 2 diabetes (T2D) via the integration of human genome-wide association studies, tissue-specific regulation of gene expression, and network modeling. We found shared gene networks between AD and T2D involved in lipid metabolism, insulin receptor signaling, adaptive immunity, complement cascade, cell cycle, PPAR signaling, and extracellular matrix. We further pinpointed key regulators of the shared networks such as *SLC15A3, NCKAP1L, FERMT3, FN1,* and *EMR1*. In a mouse study, we investigated the cell

type-specific transcriptome changes of the hippocampus and hypothalamus in the 5XFAD model under metabolic modulation via dietary challenges, namely fructose, docosahexaenoic acid (DHA), and nicotinamide riboside (NR). We identified robust cell type-specific responses to disease state in the 5XFAD model including increased expression of proteolytic and lipid transport genes which act to compensate for amyloidosis. Fructose was found to reverse these transcriptional signatures, likely impairing amyloid clearance mechanisms, which was rescued by DHA and NR. Lastly, based on the genetically informed disease subnetworks, we predict PPARγ agonists and androgen receptor agonists to be possible drugs in the prevention of AD, and based on transcriptional profiles in 5XFAD, we predict phensuximde and tankyrase inhibitors to neutralize the deleterious effects of amyloidosis.

The thesis of Jessica Aliyah Ding is approved.

Stephanie Correa

Peter J. Tontonoz

Xia Yang, Committee Chair

University of California, Los Angeles

2020

## Table of Contents

## List of Tables and Figures

**Acknowledgements**

I would like to thank my committee members Professors Stephanie Correa and Peter Tontonoz for their helpful feedback and suggestions on the thesis. I would like to thank my principal investigator Professor Xia Yang for her consistent guidance and mentorship. I would like to thank Lily Ying, Dr. Victoria Sánchez, and Professor Fernando Gomez-Pinilla for their contributions to the animal work in the single-cell study. I would like to thank Dr. In Sook Ahn and Dr. Graciel Diamante for their preparation of the data for the single-cell study. I would like to thank my lab mates, my family, and my friends for their continual support. The studies were partially funded by NIH R01 DK104363.

## 1. Introduction and Background

### Characterization of Alzheimer's disease

Alzheimer's disease (AD) is an increasingly prevalent progressive neurodegenerative disease leading to loss of memory, cognition, and executive functions. The long-standing hallmarks of AD are accumulations of extracellular amyloid-β (Aβ) plaques and hyperphosphorylated tau protein in the brain. In addition to these protein aggregates, neuronal atrophy is thought to be compounded by multiple abnormal physiological states including neuroinflammation, disrupted glucose metabolism, metal ion homeostasis, mitochondrial dysfunction, and oxidative stress[1-5]. Although extension examination of these features has been conducted in the context of AD, the causal pathogenic pathways involved in the development of AD remain elusive. Determining the etiology of AD is paramount for designing effective preventative and treatment strategies.

### Metabolic contributions to the etiology of AD

Among the potential causal factors for AD, metabolic dysregulation is an underexplored aspect. Over the past decade, epidemiological and experimental evidence has accrued supporting a strong connection of metabolic diseases with AD development. Insulin resistance and loss of glucose regulation are emerging as important pathogenic mechanisms for AD[6]. Metabolic diseases compromise brain integrity[7], promote cognitive and emotional disturbances[8], and increase vulnerability to AD[9-12]. Individuals with diabetes have lower cognitive function and twice the risk for developing AD compared to healthy individuals[13]. The high incidence of AD comorbidity with metabolic syndrome suggests shared molecular mechanisms underlying these ailments[14]. Alterations in systemic metabolism have a potent influence on brain plasticity and function, and there is strong evidence to suggest that a loss of the ability to regulate systemic metabolism is a hallmark of AD pathogenesis[15,16].

**Introduction to systems biology projects**

In order to investigate the role of metabolism in AD, I carried out two projects building on systems biology concepts and approaches. System biology aims to map molecular interactions within and between cells or tissues to offer comprehensive network views of physiology or disease pathogenesis[17]. In the first project, we identify shared genetic mechanisms between AD and type 2 diabetes (T2D) using integrative analysis of human multi-omics datasets. In the second project, we delineate cell-type specific alterations in amyloidosis and the modulatory effects of fructose, docosahexaenoic acid (DHA), a dietary omega-3 fatty acid, and nicotinamide riboside (NR), a modulator of mitochondrial function and a precursor of NAD+, in the 5XFAD mouse model of AD. In this multi-faceted approach, we find causal mediators of AD pathogenesis and prioritize those shared with metabolic diseases and explore the effect of nutritional interventions on AD pathways and pathology.

To understand the causal mechanisms of AD and its connection to metabolic diseases, we investigated the shared genetic mechanisms between AD and T2D, a common metabolic disorder characterized by hyperglycemia and impaired insulin signaling. AD and T2D are complex, polygenic diseases, and we have seen success in identifying numerous risk loci through genome-wide association studies (GWAS)[18-21]. However, meaningful functional molecular mechanisms connecting these diseases have not been interpreted from these studies. In our study, we conduct a rigorous interpretation and integration of GWAS data from AD and T2D with functional genomics data to identify disease genes involved in coherent pathways or functional modules and model the perturbations in gene regulatory networks contributing to pathogenesis. In identifying these downstream effectors and key regulatory genes, we bridge the gap from risk loci to disease manifestation and provide candidate genes for meaningful drug predictions.

Metabolic dysregulation has been observed in mouse models of AD[22], yet the causal nature of the metabolic alterations and the underlying molecular pathways are poorly

understood. Modulating the metabolic aspects of AD models using dietary perturbations serves as an effective way to test causality of metabolism in AD development[23]. Additionally, there is considerable cell type heterogeneity in the brain in which each cell type has specific functions and responses to stressors. Single-cell RNA sequencing (scRNAseq) is enabling the discovery of molecular mechanisms of complex diseases at single cell resolution. Therefore, we aim to decipher the cell type-specific pathways altered in the hippocampus (involved in AD pathology) and hypothalamus (involved in metabolic regulation) in a mouse model of AD, survey the effect of inducing metabolic syndrome using a high fructose diet in the context of Aβ accumulation, and test the potential of DHA and NR to ameliorate fructose-induced changes in the AD model.

Lastly, we employ drug repositioning informed by shared genetic mechanisms between AD and T2D and by the cell-type specific mechanisms of AD to identify drugs that have the potential to prevent the onset of AD pathogenesis or ameliorate AD symptoms.

## 2. Shared Mechanisms between Type 2 Diabetes and Alzheimer's Disease via Integrative Genomics Analysis

### Introduction

AD and T2D are among the most prevalent ailments of the aging population globally. AD is the fifth leading cause of death of individuals older than 65 in the United States[24] and 463 million adults worldwide are diagnosed with T2D[25]. Compelling evidence demonstrates that insulin resistance and metabolic syndrome may be casual for AD. T2D patients often exhibit cognitive impairment and have a 50-60% increased risk for AD compared to healthy individuals[26]. Increased blood insulin levels have been shown to exacerbate markers of AD including tau phosphorylation, Aβ accumulation, and neuronal death[27,28]. Though consumption of glucose by the brain is largely independent of insulin, insulin receptors are expressed widely throughout the brain, demonstrating a crucial role of insulin in a variety of functions such as

learning and memory in the hippocampus[29]. The link between insulin resistance and AD has been so frequently reported that AD is colloquially referred to as Type 3 diabetes, or diabetes of the brain.

Despite the observed connections between AD and T2D, whether the two diseases share common causal mechanisms remains unclear. One way to tackle this question is through comparing the genetic risk loci associated with these diseases identify in genome-wide association studies (GWAS). Indeed, previous studies investigated shared genetic factors in AD and metabolic disorders at the level of genetic variants represented by single nucleotide polymorphisms (SNPs), revealing limited overlaps[30-32]. However, as demonstrated in our previous between-disease or between-species comparison studies, it is unlikely that pathogenic overlaps are at the individual variant or gene levels, but more at the pathway or networks levels[33,34]. To date, none of the previous studies have utilized a network-based approach to fully understand network level similarities between AD and T2D.

Network modeling of multi-omics data via systems biology is increasingly recognized as a powerful means to understand complex diseases and traits such as AD and T2D. This approach is built on the increasing scientific evidence supporting a network concept of physiological processes, where molecular entities such as genes and proteins interact in non-random networks in a tissue-specific manner, with central “hubs” regulating large numbers of “peripheral” molecules to perform biological functions; molecular networks between tissues also interact to help maintain systems level homeostasis. The network concept aligns with the increasingly recognized “omnigenic disease model”[35], which states that almost all genes in networks contribute to disease development with varying degrees of effect sizes and central hub genes likely have stronger effects whereas peripheral genes exhibit moderate to weaker effects. Therefore, it is essential to understand the perturbed tissue-specific networks of diseases and use the networks to guide the identification of more important therapeutic targets and drug candidates.

We have developed an open-access computational pipeline, Mergeomics[34,36], to facilitate such omics integration and disease network modeling. Importantly, Mergeomics utilizes the full spectrum of multi-omics datasets, rather than merely the top disease association signals, to uncover gene networks and molecular pathways within and between tissues that can explain much higher genetic heritability than traditional tools. Our approach follows the principles of the "omnigenic" model of inheritance, which describes the genetic architecture of complex traits to be comprised of hundreds of gene contributions across the entire genome[35].

Here we discuss genetically informed mechanistic links between AD and T2D in the form of tissue-specific networks that have been previously underreported, identify key regulators underlying AD and T2D disease subnetworks, and propose potential drugs for the treatment of AD. To our knowledge, this is one of the first efforts utilizing a gene regulatory network approach to reveal shared mechanisms between AD and T2D and identify functional key drivers and drugs targeting the shared networks.

## Methods

### *Overall Study Design*

As illustrated in **Figure 1**, we retrieved the canonical pathways and coexpression gene modules that were significantly enriched for AD and T2D GWAS loci separately and consider only those gene sets that are replicated in at least two of the GWAS studies of the same disease. We then used the shared AD and T2D pathways to create shared AD and T2D subnetworks and pinpoint key regulators based on the shared disease subnetwork topology. The subnetwork genes are then used for drug repositioning analysis.

### *GWAS Datasets*

Three genome-wide association studies (GWAS) of T2D were obtained from the Diabetes Genetics Replication and Meta-analysis (DIAGRAM) consortium stage 1[37], UK Biobank[38], and a multi-ethnic study from Wojcik et al.[39]. The DIAGRAM consortium stage 1 GWAS was a meta-analysis of 12,171 cases and 56,862 controls taken from 18 GWAS studies of European ancestry that used Illumina and Affymetrix SNP genotyping platforms as well as Metabochip. Genotype data were imputed to the 1000 Genomes reference panel. These studies include Atherosclerosis Risk in Communities (ARIC), Mt. Sinai BioMe BioBank (BioMe), Diabetes Gene Discovery Group (DGDG), Diabetes Genetics Initiative (DGI), Wellcome Trust Case-Control Consortium (WTCCC), and others. For UK Biobank, there were 21,147 cases and 434,460 controls. The data was imputed to the Haplotype Reference Consortium. For the Wojcik et al. study, samples were taken from the Population Architecture using Genomics and Epidemiology (PAGE) study and comprised 5,971/9,630 African American cases/controls, 4,135/16,345 Hispanic/Latino cases/controls, 2,004/2,572 Asian ancestry cases/controls, 1,534/2,017 Native Hawaiian ancestry cases/controls, 167/452 Native American ancestry cases/controls. These samples were genotyped on the Multi-Ethnic Genotyping Array developed by the PAGE study. Genotype data were imputed to the 1000 Genomes reference panel.

Two sets of AD GWAS summary statistics were used. The Jun et al. study[40] included datasets from the Alzheimer's Disease Genetics Consortium (ADGC) and the International Genomics Alzheimer's Project (IGAP). The ADGC subjects were comprised of 13,100/13220 European cases/controls, 1,472/3,511 African American cases/controls, 951/894 Japanese cases/controls, and 51/64 Israeli-Arab cases/controls. Genotyping was done with Illumina and Affymetrix sequencing platforms. Genome imputation was performed using the 1000 Genomes panel. In IGAP, there were 5,813 cases and 20,474 controls after excluding data from ADGC. The second AD GWAS was the UK Biobank AD study[41] which utilized a proxy-phenotype approach in which participants were asked if their mother or father suffered from AD. Inclusion

criteria included participants with parents over 60 years of age. There were 27,696 maternal cases with 260,980 controls and 14,338 paternal cases with 245,941 controls. The majority (90%) of participants were genotyped using the UK Biobank Axiom Array and the others with UK BiLEVE Axiom Array.

*SNP to gene mapping methods*

Tissue-specific expression quantitative trait loci (eQTL) and splicing quantitative trait loci (sQTLs) were used to map gene variants to changes in expression levels and changes in alternative splicing. All 49 sets of human eQTLs and sQTLs were taken from the Genotype-Tissue Expression project (GTEx) (version 8)[42], representing genetic regulation of gene expression in 49 different human tissues. Functional information from the RegulomeDB database (version 1.1; www.regulomedb.org) based on the ENCODE (Encyclopedia of DNA Elements) project[43] were collected to map SNPs within regulatory regions (promoters and enhancers) to the corresponding genes. Distance based mapping was also used with a SNP being mapped to a gene within a 50kb distance. For each GWAS set, SNPs were mapped to genes using tissue-specific eQTLs or sQTLs, ENCODE functional elements, and 50kb distance.

*Canonical pathways and data-driven coexpression modules*

We curated 1,891 knowledge-driven canonical pathways from KEGG[44], Reactome[45], and BioCarta[46], and complemented the pathways with 9,315 coexpression data-driven gene modules (each module contains highly correlated or coregulated genes) derived from version 7 GTEx expression matrices of 24 disease relevant tissues using WGCNA[47] and MEGENA[48]. As AD and T2D pathology includes components of dysregulated metabolism, immune system, endocrine function, and cognition, we included metabolic tissues such as adipose, colon, liver, and pancreas, endocrine organs such as adrenal gland, pituitary and thyroid, immune-related tissues such as spleen and whole blood, circulatory tissues such as aortic and tibial artery, and

nervous system tissues such as tibial nerve, cerebellar hemisphere, cerebellum, cortex, hippocampus, and hypothalamus. Tissue-specific coexpression modules were tested with the corresponding tissue eQTL/sQTL mapping method.

*Marker set enrichment analysis (MSEA)*

The AD/T2D GWAS datasets, knowledge-driven pathways and data-driven co-expression modules, and functional genomics described above were used in MSEA, a component of Mergeomics[34], to determine if any of the pathways/modules demonstrate significant genetic association with AD and T2D. Before performing MSEA, we preprocessed the GWAS datasets for AD and T2D to adjust for linkage disequilibrium (LD) structure. We pruned SNPs using a LD cutoff of $r^2<0.5$ to remove redundant SNPs. Disease association of pathways and coexpression modules was tested using a chi-square-like statistics implemented in MSEA to derive enrichment p values[34]. We adjusted the enrichment p values by using the Benjamini-Hochberg method to estimate false discovery rate (FDR). Pathways or coexpression modules were considered significant if FDR<0.05.

*Key driver analysis (KDA)*

To identify key regulatory genes (termed as Key Drivers, KDs) of the significant pathways and coexpression modules that contribute to both T2D and AD, we performed KDA. Bayesian networks (BNs), which delineate gene-gene regulatory interactions, were used for the KDA and were constructed using RIMBANet[49] which uses gene expression data, transcription factor information, and eQTLs to create probabilistic gene regulatory networks. The sources used to construct these BNs are listed in **Table 1**. In KDA, member genes of the shared pathways and coexpression modules are used to query Bayesian regulatory networks and KDs were identified by those having network neighborhoods enriched for shared AD and T2D module genes based on network topology. Enrichment was assessed with chi-square-like

statistics, and Bonferroni-corrected p<0.05 was used to determine the significance of KDs. The regulatory subnetworks for a subset of KDs were visualized using Cytoscape[50].

*Drug repositioning using Pharmomics*

Pharmomics[51] is comprised of genomic footprints derived from meta-analysis of microarray and RNA sequencing data relevant to drugs from tissues and cells from human, mouse, and rat samples in GEO, ArrayExpress, TG-GATEs and drugMatrix data repositories. Drugs are identified based on overlaps between the AD-T2D gene networks and the drug database gene signatures using the Jaccard score method which assesses the significance of the overlap.

## Results

*Shared pathways and modules between AD and T2D*

Among the 1,891 pathways and 9,315 coexpression modules tested, 199 canonical pathways and 77 coexpression modules were found to be enriched for GWAS signals for both AD and T2D which were replicated across all GWAS studies at FDR<5%. These were determined as the shared pathways and modules between AD and T2D. As some of the pathways and modules exhibited overlaps in their gene members, we merged the 199 pathways and 77 modules into 39 nonoverlapping supersets using the criteria of >30% gene overlap and p<0.05 based on Fisher's exact test. Representative pathways of these supersets are shown in **Table 2**.

The proportion of significant pathways and coexpression modules from the different SNP-to-gene mapping methods used in this study were similar between AD and T2D, meaning no particular mapping method was markedly more or less informative in one disease compared to the other (**Figure 2**). Subcutaneous adipose and tibial nerve eQTLs yielded the greatest

amount of significantly enriched modules. A difference between AD and T2D was liver eQTLs informing gene modules for T2D but not for AD, though there were 12 significant modules from the UKB AD study from liver eQTLs, but none were replicated in the Jun et al. AD study. Another marginal difference was adrenal gland, pancreas, and thyroid sQTLs informing AD gene modules but not T2D gene modules. In the case of thyroid sQTLs for T2D, significant signals from the DIAGRAM study were not replicated in either the UKB T2D study or the Wojcik et al. study.

Below we discuss select pathways and their constituent genes that were shared between AD and T2D. Notably, many were related to metabolic, immune, cell cycle, and endocytosis functions. While the Wojcik et al. informed on many pathways that were replicated in other T2D studies and thus added on to the list of replicated T2D pathways, none of the genes that were members of enriched pathways were mapped from loci that had p-values less than 0.01. The discussed genes below are replicated across the other four GWAS studies (two AD and two T2D) with a p-value of less than 0.001, unless stated otherwise.

Pathways that were consistent across multiple SNP mapping methods (distance, ENCODE, and tissue-specific eQTLs/sQTLs) included those relating to immune function such as the adaptive immune system, MHC mediated antigen processing, and complement cascade. Inflammation is a well described pathogenic feature in both AD and T2D[2,52,53]. The genes that were replicated in all four GWAS studies in the immune functional category include *MICA*, *MICB*, *TAP2*, *PSMB9*, and *PSMC5*. *MICA* and *MICB* encode the MHC Class I chain related proteins that serve as ligands for natural killer cells[54]. These genes have linked to Type 1 diabetes, and *MICB* protein expression in the prefrontal cortex has been observed to be increased in the progression of AD[55], but detailed discussion of their role in T2D and AD is lacking. More recently, infection caused by viruses and bacteria has been hypothesized to spur the development of AD and T2D[56-58]. *PVRL2*, a member of genes related to high-density lipoprotein cholesterol (HDLC) and replicated across all four GWAS studies, encodes a

cholesterol-responsive membrane glycoprotein that acts as an entry point for certain strains of herpes simplex virus and pseudorabies virus[59], although this association may be in linkage disequilibrium with *APOE*[60]. V-ATPase genes, which were also replicated across the four GWAS studies and members of many of the shared pathways, are involved in viral entry into the cell[61]. These may be among the genetic variants that are posing higher susceptibility to infection and thus to development of the disease in AD and T2D patients.

Other immune related pathways shared between AD and T2D include RIG-I/MDA5 mediated induction of IFN-alpha/beta pathways, Toll-Like Receptors Cascades, TRAF6 mediated NF-κB activation, and advanced glycosylation endproduct receptor signaling. *AGER* was a mapped gene for all four GWAS studies through many different SNP mapping methods and was a member of these shared pathways. *AGER* encodes advanced glycosylation end-product specific receptor, also known as RAGE, which is part of the immunoglobulin superfamily. Genetic association of *AGER* to T2D and its vascular complications is well documented[62]. Hyperglycemia in T2D accelerates the production of advanced glycation end-products (AGEs), which stimulate vascular inflammation and oxidative stress upon binding to AGER[63]. Aβ is also a ligand of AGER and serves as the gateway for Aβ from the blood to the brain via the blood brain barrier[64].

Expectedly, gene sets relating to metabolic traits and lipid metabolism were also consistent between AD and T2D across SNP mapping methods. These included gene sets for coronary heart disease, HDLC, triglyceride biosynthesis, and glycerolipid metabolism. Genes in these metabolic categories included *TOMM40*, *AGPAT1*, *ELOVL5*, and *GPAM*. *GPAM* expression was shown to be downregulated in CA1 neurons of the hippocampus[65] and chromatin accessibility of the *GPAM* gene was increased in saturated fatty acid treated adipocytes in a BMI gene-environment study[66]. *AGPAT1* encodes an enzyme that converts lysophosphatidic acid (LPA) into phosphatidic acid which is involved in lipid biosynthesis. *Agpat1* null mice have severe metabolic and neurological complications such as low body

weight and plasma glucose levels, decreased numbers of hippocampal neurons, and lethality before weaning[67]. These results provide support for the role of AGPAT1 in both glucose homeostasis and nervous system function. Additionally, LPA-mediated neurite retraction increases tau phosphorylation, a hallmark of AD[68].

The Reactome pathways 'Signaling by Insulin receptor' (R-HSA-74752) and 'Insulin receptor recycling' (R-HSA-77387) was significant in both AD and T2D, although other insulin-related pathways such as the KEGG 'Insulin signaling pathway' (hsa04910), BioCarta 'Insulin Signaling pathway', were specific to T2D. These pathways reflect different aspects of insulin signaling and for the most part consist of different genes as these pathways were not merged at the 30% overlap threshold. The insulin pathways that were shared between AD and T2D were distinguished from the T2D specific insulin pathways with its member genes encoding several vacuolar ATPases (V-ATPases), representing the process of endosomal acidification, and fibroblast growth factors, shown to increase insulin sensitivity[69]. The specific mapped genes from AD and T2D GWAS loci in this pathway include *ATP6V1G2*, *ATP6V0A1*, *ATP6V0D1*, *FGF2*, and *FGF7*. Genes enriched in the T2D specific insulin pathways included *IRS1*, *FLOT1*, *FBP2*, *HK1*, *MAP2K1*, and *RAF1*.

In insulin signaling, the activated insulin receptor is internalized via endosomes, and V-ATPases residing in these endosomes are responsible for H+ acidification which leads to the degradation of insulin and dephosphorylation of the receptor and its re-incorporation with the plasma membrane. V-ATPases also maintain the acidification of other intracellular compartments such as lysosomes and regulate synaptic transmission[70,71]. *ATP6V0A1*, which encodes the ATPase V0 a1 subunit, is shown to mediate the fusion of phagosomes and lysosomes during microglial phagocytosis in addition to its proton pump function[72]. Thus, abnormalities in *ATP6V0A1* could incite microglial neurotoxicity. ATPase V1 G2 subunit, encoded by *ATP6V1G2*, the most significant and replicated V-ATPase gene, is neuron-specific, and its role in disease is unknown.

V-ATPases also participate in transferrin endocytosis and recycling which was a pathway significantly enriched in both AD and T2D and informed by tibial nerve eQTLs. Transferrin is a serum glycoprotein that transports iron into cells through endocytosis after binding to its receptor. Acidification by V-ATPases of the endosome that fuses with a vesicle containing the transferrin-receptor complex allows for release of iron and also for transferrin to remain associated with its receptor. Transferrin is recycled back to the plasma membrane bound to its receptor, and the neutral pH at the plasma membrane decreases its affinity for the receptor, and the receptor is released back into circulation[73]. A defect in V-ATPases could disrupt the balance of iron and transferrin which has been seen in AD. Transferrin has been shown to decline with AD progression in the blood[74,75], and brain iron levels increase with age and are even greater in neurodegeneration[76]. High iron levels are also linked to T2D[77]. In addition, iron accelerates oxidation of glucose and fructose by AGEs and Aβ aggregation[78,79].

Cell cycle control genes such as *CDKN2A* and *CDKN2B* which were constituents of the gene sets for coronary heart disease and T2D were also replicated across the four GWAS studies for AD and T2D. *CDKN2A* and *CDKN2B* are tumor suppressor genes that encode proteins that inhibit cyclin dependent kinases responsible for the G1/S transition. The association of the *CDKN2A*/*B* loci to T2D has been reported numerous times, and these genes have been hypothesized to play a role in beta cell mass and proliferation[80]. The genetic association of *CDKN2A/B* to AD has been described[81,82], and the protein products of *CDKN2A*, p16, an inhibitor of cyclin-dependent kinase 4, has been shown to be increased in AD brains and localized to neurofibrillary tangles and plaques[83,84], and whole blood expression of CDKN2A was higher in pre-clinical AD versus controls[85]. At terminal differentiation, neurons normally remain in G0 and transition to G1 in oxidative stress conditions; this cell cycle re-entry is thought to lead to pathogenic outcomes in AD[86], and *CDKN2A/B*, among other genes that were enriched for the ‘cell cycle’ pathway, may be involved in this abnormal neuronal response.

The shared pathway 'Phase I functionalization' comprised several genes that are underexplored in the context of AD and T2D. *CYP21A2* was highly significant across the four GWAS studies. *CYP21A2* encodes 21-hydroxylase which is required for the synthesis of cortisol and aldosterone. 21-hydroxylase modulates androgen levels as the compounds that make up cortisol and aldosterone can also be converted into androgen. For example, 21-hydroxylase deficiency leads to an increase in androgen levels[87]. Although *CYP21A2* has not been functionally tied to AD, androgens are thought to be negative regulators of Aβ production[88]. This may explain in part the higher incidence of AD in females than in males as females have less circulating androgen levels. A 21-hydroxylase deficiency has been loosely connected to types of diabetes in certain case studies[89,90], and sex hormones have complex relations to the risk of T2D[91]. Other replicated genes in AD and T2D GWAS include other members of the cytochrome P450 family such as *CYP2D6* and *CYP4F11* and alcohol dehydrogenase genes such as *ADH1A*, *ADH1C*, and *ADH4*. Cytochrome P450 enzymes participate in xenobiotic metabolism and help to produce cholesterol and lipids. Alcohol dehydrogenases have been linked to both AD and T2D[92,93].

Other shared pathways include 'notch signaling' informed by combined peripheral and subcutaneous adipose eQTLs, 'lectin induced complement pathway' informed by all combined and peripheral combined eQTLs, and 'regulation of lipid metabolism by peroxisome proliferator-activated receptor alpha (PPARalpha)' informed by peripheral combined eQTLs. Notch, complement, and PPAR pathways have been implicated before in both AD and T2D[94-99]. Our study offers genetic evidence and thus causal implications for these pathways.

*Disease-specific pathways and modules*

Among the 344 canonical and 169 coexpression that were significantly enriched for AD GWAS signals in at least one SNP-to-gene mapping method, 150 canonical pathways and 99 coexpression modules were specific to AD (i.e., no enrichment for T2D GWAS signals). The AD

specific gene sets were merged into 119 nonoverlapping supersets, representing immune function, protein folding, oxidative phosphorylation, retinoid metabolism, RNA processing, synaptic transmission, vesicular transport, and cell-cell junction organization (representative pathways shown in **Table 3**). Expectedly, pathways relating to the nervous system were specific to AD. RNA processing is also specific to AD and have been discussed, especially in the context of splicing[100,101].

The genes that informed the enrichment of these AD-specific pathways include *PVR*, *MICB*, *CD55*, *CD33*, *CR1*, *SKIV2L*, *ATP6V1G2*, *APOC2*, *APOE*, *BIN1*, *PICALM*, *GEMIN7*, *ADAM10*, *PSMB8*, *ACHE*, *POLR2E*, *STX1B*, *CDH4*, and *PVRL2*. There were 170 replicated AD specific genes at a p-value less than 0.001. Several of the same highly significant genes are listed here and in the shared AD and T2D genes because these genes participate in many different replicated pathways. In addition, we only discuss genes mapped from loci that passed a p-value of 0.001 which represented only 6.4% of all loci mapped to genes within the AD-specific pathways or coexpression modules.

The AD specific genes involved in RNA processing, splicing, and translation such as *SKIV2L*, *POLR2E*, and *STX1B* have no known direct connections to the development of AD as experimental evidence of their roles is lacking. Genetic variants in *ACHE* (acetylcholinesterase) associated with AD falls in line with current evidence of cholinergic deficits in early AD[102]. *STX1B* plays a role in exocytosis of synaptic vesicles. This and other pathways and genes involved in neuronal transmission provide evidence that genetic determinants of AD do involve disruptions of central nervous system functions, but we believe these can be compounded by metabolic deficits or vulnerabilities to brain dysfunction caused by genetic variants can be triggered or exacerbated by metabolic abnormalities.

Among the 261 canonical pathways and 113 coexpression modules that were significantly enriched for T2D GWAS signals in at least one SNP-to-gene mapping method, 60 canonical pathways and 44 coexpression modules were specific to T2D (i.e., no enrichment for

AD GWAS signals). The T2D-specific gene sets were merged into 24 nonoverlapping supersets (representative pathways shown in **Table 4**). These T2D specific pathways included diabetes related traits such as HbA1c levels and body mass index (BMI), insulin-related pathways such as 'Insulin signaling pathway' from KEGG and BioCarta, 'regulation of beta-cell development', 'incretin synthesis, secretion, and inactivation', 'Regulation of gene expression in beta cells', and 'Synthesis, Secretion, and Inactivation of Glucose-dependent Insulinotropic Polypeptide (GIP)'. Although 'protein folding' was AD specific, the 'unfolded protein response' was specific to T2D, comprising different gene enrichments including *SSR1*, which encodes translocon-associated protein subunit alpha, involved in folding of translocated proteins in the endoplasmic reticulum membrane and serves as a connection between insulin demand and beta cell failure[103]. 'Zinc transporters' was also significantly enriched for T2D GWAS by distance mapping which comprised many genes of the solute carrier family including *SLC20A8*, *SLC30A5*, *SLC39A10*, and *SLC39A5*. Zinc is thought to maintain insulin sensitivity and glycemic control[104], and genetic variants in these zinc transporters may lead to its dysregulation. Zinc is hypothesized to be neurotoxic at high concentrations in the brain and has been proposed to promote AD pathology [105,106]. This may be one of the pathogenic pathways linking T2D to the development of AD. Aquaporin-mediated transport was also a T2D specific pathway, and aquaporins are thought to maintain insulin signaling[107] and be involved in Aβ clearance[108,109].

There were 647 replicated genes unique to T2D, which is much more than that of AD. These include *EHHADH*, *FABP4*, *FADS2*, *LPL*, *SCD5*, *ACSL1*, *ANK1*, *CDKAL1*, *FLOT1*, *HK1*, *IRS1*, *SLC2A2*, *HNF1A*, and *HNF4B*.

*Construction of shared AD and T2D disease network and identification of key drivers*

Next, we sought to define the interactions between the diverse processes shared between AD and T2D and pinpoint integral key regulators in gene regulatory networks. We first retrieved two Bayesian networks, one representing a cross-tissue network combined from

numerous tissue-specific networks and one representing a brain network combining networks from various brain regions (**Table 1**). Accordingly, we focus on the shared pathways and modules informed by combined peripheral eQTLs across 36 tissues and combined brain eQTLs across 13 brain regions. This comprehensive approach was used to investigate all possible gene interactions, although we acknowledge the loss of tissue and brain region specificity. A subnetwork representing a subset of the key drivers described in the next section and exemplifying the molecular interactions between diverse pathways with high representation from lipid metabolism and immune function genes is shown in **Figure 3**.

Querying the cross-tissue Bayesian network using 39 nonoverlapping modules from combined peripheral eQTLs shared between AD and T2D comprising 3,670 genes, we identified top key drivers involved in lipid metabolism and cholesterol transport (*FASN*, *THRSP*, *ELOVL5*, *AACS*, *DGAT2*, *LDLR*, *APOC2*, *INSIG1*, *ACSL1, AGPAT2*), immune regulation (*NCKAP1L*, *CFI*, *CTSK*, *PTPRC*, *SYK*, *HCK*, *ITGAL, FERMT3, TYROBP, KNG1, MYO1F, FCER1G*), extracellular matrix (*COL1A1*, *COL1A2*, *PCOLCE*, *FBN1*, *COL3A1*, *ADAMTS2*, *COL6A3*, *LOXL1*), peroxisome (*ACSL1*, *EHHADH*, *FDPS*, *IDI1*, *PEX11A*, *EPHX2*, *FADS1*), PPAR signaling (*ACSL1*, *HMGCS1*, *FDFT1*, *PEX11A*, *CPT2*, *HMGCR*, *HMGCS2*), glycolysis (*GYS2*, *COL5A1*, *PYGL*, *NSDHL*, *ALDOB*, *IDH1*, *DCN*, *VCAN*), fatty acid oxidation (ECHS1, ACADVL), and mitochondrial function (ETFDH).

Querying the brain network using 4 nonoverlapping modules informed by brain eQTLs shared between AD and T2D comprising 599 genes, yielded 56 significant (FDR<0.05) key drivers. The top KDs included those involved in the immune system (*IFITM2*, *LY86*, *FYB*, *HLA-DRB1*, *HLA-DQA1*, *ITGB2*, *GBP1*, *IFITM1*), complement and coagulation cascade (*SERPING1*, *THBD*, *C1QC*, *VWF*, *C1QA*), extracellular matrix (*COL1A2*, *COL3A1*, *VWF*, *COL1A1*), and glycosaminoglycan metabolism (*FMOD*, *BGN*, *LUM*).

There were 37 KDs shared between the peripheral network and brain network and included mainly extracellular matrix and immune function genes (*COL1A1*, *COL1A2*, *PCOLCE*,

*COL3A1*, *LOXL1*, *FMOD*, *FN1*, *BGN*, *SERPING1*, *LUM*, *EFEMP1*, *LY86*, *DCN*, *ANXA2*, *FYB*, *CXCL12*, *CYP1B1*, *ISLR*, *ITGB2*, *SLC13A4*, *TREM2*, *HLA-DQA1*, *EMP3*, *VWF*, *FOXC1*, *THBD*, *CRISPLD2*, *C1QA*, *LRG1*, *NID1*, *C1QC*, *HLA-DRB1*, *IFITM2*, *GBP1*, and *HVCN1*). Many lipid metabolism, transmembrane transport (*SLC15A3*, *SLC22A1*, *ABCG1*, *APOA1*, *ATP6V1A*, *SLC25A10*), and some inflammatory (*EMR1*, *LCP2*, *TLR2*, *IL1B*, *CCL5*, *TIMP1*, *IL10RA*, *RGS1*, *LDLR*, *CCL2*, *IL6*, *BTG2*, *CD14*) KDs were specific to the peripheral network. Brain specific KDs included *TAGLN*, *ACTA2*, *FAS*, *OSMR*, and *CXCL16*.

*Drug repositioning based on shared AD and T2D disease network*

We used the shared cross-tissue peripheral network comprised of the top key drivers and their neighboring genes to identify drugs whose gene signatures match with the network. Top predicted drugs were ‘dementia therapeutic agent’, ‘NMDA receptor antagonist’, ‘Antihyperlipidemic’ , ‘Antidiabetic’, ‘Peroxisome proliferator-activated receptor gamma agonist’, 'Memantine’, ‘Androgen receptor antagonist’, ‘Antihyperlipidemic’, ‘Estrogen receptor agonist’, ‘aldosterone’, ‘Toll-like receptor agonist’, ‘Rosiglitazone’ (an antidiabetic drug), Fenofibrate (used to reduce cholesterol and triglycerides), and ‘Baricitinib’ (an inhibitor of janus kinases JAK1 and JAK2). When only using the key drivers, ‘androgen receptor antagonist’, ‘Peroxisome proliferator-activated receptor gamma agonist’, ‘antidiabetic’, and ‘triglyceride synthesis inhibitor’ were among the top predicted drugs.

Both androgen receptor antagonist and androgen receptor agonist were predicted drugs. This discrepancy is expected given the lack of incorporation of the directionality of the specific changes that the risk loci has on gene expression levels or protein activity levels (increased or decreased gene expression or protein activity). Interestingly, androgen deprivation therapy is a risk factor for AD[110]. This drug prediction also connects to our discussion of the proposed effect of *CYP21A2* on AD and T2D.

From the brain top key driver network, top predicted drugs include Vemurafenib, an inhibitor of the B-Raf enzyme, Nicotine, an agonist for nicotinic acetylcholine receptors, Methylphenidate, used to treat attention deficit hyperactivity disorder, Etanercept, a TNF blocker, 'TNF receptor antagonist', Enzalutamide, a nonsteroidal antiandrogen medication, Medroxyprogesterone, a synthetic pregnane steroid, and Bicalutamide, an antiandrogen.

**Discussion**

In this comprehensive multi-omics integrative study of AD and T2D leveraging GWAS and tissue-specific gene regulation and networks, we found a large number of diverse pathways shared between AD and T2D, reflecting their complex disease biology and emphasizing the importance of a systems level perspective in deciphering genetic disease topologies. Subsequently, we used these gene sets to query Bayesian gene regulatory networks to generate disease subnetworks which were composed of cell cycle, lipid metabolism, extracellular matrix, and immune genes. Among the top predicted drugs were antidiabetic drugs, immune modulators, PPAR agonists, dementia therapeutics, steroid hormone receptor agonists and antagonists, and anticancer drugs. As these drugs were predicted based on genetically perturbed gene networks, they have the potential to be preventative drugs for AD.

Most of the aforementioned genes in the AD and/or T2D pathways or coexpression modules are those that are replicated in the two AD studies and at least two of the T2D studies. The SNPs that were mapped to those genes have p-values that are less than $10^{-3}$ with most around $10^{-5}$. While most do not pass standard GWAS significance ($5 \times 10^{-8}$), rarely do the majority of significant SNPs passing this threshold explain a large proportion of the heritability of a trait[111]. We emphasize again the utility of finding functional groups of genes and delineating their interactions which collectively may provide the missing heritability commonly seen in GWAS studies[112,113].

Genetic variants manifest differential changes in specific tissues and cell types[114]. The amount of significantly enriched pathways across many different tissue-specific eQTLs in AD such as adipose, artery, colon, esophagus, muscle, pancreas, and thyroid and similar distribution of numbers of modules informed by each tissue in T2D (**Figure 2**) provides evidence that systemic alterations, not just in the brain, contribute significantly to AD. We recognize the lack of tissue and cell type specificity in our current key driver and drug repositioning analyses due to limitations in available networks and drug perturbation databases. For future studies, we plan to parse the specific tissue and cell type gene networks to investigate common and unique key drivers and to make more informed selection of drug compounds and drug combinations for repositioning. In addition to differential tissue and cell type contexts within an AD or T2D patient, heterogeneity among AD and T2D subtypes reflecting differing disease biology must also be considered. In general, this is a challenge in binary GWAS studies of complex disease. In our study, we prioritize common mechanisms between AD and T2D as informed by GWAS across different study populations and tissue-specific mapping methods, and we hope to refine our analyses in the future.

Here we not only confirm the genetic basis of several pathogenic pathways such as the adaptive immune system, complement cascade, cell cycle, advanced glycosylation end product receptor signaling, and lipid metabolism underlying both AD and T2D but also discuss previously unexplored shared processes and genes such as *AGPAT1*, *CYP21A2*, *ATP6V1G2*, endosome acidification, and viral entry genes such as *PVRL2* and V-ATPases.

## 3. Multi-Tissue Single-Cell Level Understanding of Alzheimer's Disease Points to the Therapeutic Potential of Nutritional and Metabolic Modulation

### Introduction

Effective treatment for Alzheimer's disease (AD) is not yet available and the main causative factors for AD pathology remain elusive. An important yet underexplored aspect is that disturbances in vital interactions among different cell types across many brain regions are fundamental determinants of AD pathogenesis. Disruptions in key brain regions such as the hippocampus and frontal cortex, critical for cognition and behavior, are well-known hallmarks of AD. Emerging evidence also supports a potential role of the hypothalamus in driving AD pathology, as Aβ and tauopathy occur in the hypothalamus before the onset of cognitive symptoms[115]. Although neurons are heavily affected by AD pathology, it is well-accepted that neuronal function is fully dependent on the function of glial cells such as astrocytes, microglia, and oligodendrocytes within each brain region. In particular, normal brain function and homeostasis involve the orchestrated participation of numerous cell types, and malfunctions in specific cellular and molecular interactions determine abnormal Aβ deposition, neurofibrillary tangle formation, and inflammation which result in neurodegeneration. Therefore, it is crucial to delineate the alterations in specific cell types and cell-cell communications in different brain regions that underlie AD pathogenesis. Our current understanding of AD at this resolution remains limited.

The dynamic interaction between the periphery and brain enables metabolic alterations to influence the function of neurons and glial cells and their interactions. The surge in metabolic disorders resulting from the rise in consumption of high caloric foods[116] accounts for over 40% of the U.S. population being diabetic or pre-diabetic[117]. Fructose is widely consumed in soft drinks and processed foods and is gaining recognition as a major contributor to the current epidemic of metabolic disorders in humans[118-120]. Although fructose has been found to alter brain activities[121-123], surprisingly very little is known about the influence of fructose in AD.

Given that metabolic dysfunction is becoming a well-accepted risk factor for AD and the observed perturbations in energy metabolism in the 5XFAD AD model[124,125], we hypothesize that the mitochondria activator NAD+ can influence genes and pathways affected in AD to

promote AD regression. In addition, we have previously shown that DHA can offset the complex metabolic effects of fructose in animal models of metabolic and brain disorders[126]. The various positive actions of DHA to improve insulin resistance and act at several cellular and molecular levels in the brain such as synaptic plasticity, plasma membrane integrity, and neuronal signaling[127] suggest that DHA is particularly suitable to defend against the broad pathology of AD. We hypothesize that that NAD+ and DHA treatments have complementary actions that lead to the normalization of cell-type specific gene regulatory mechanisms necessary for neuronal and glial function, metabolic fitness, and cognition.

In this study, we dissect cell-type specific vulnerability and complex molecular and cellular interactions involved in AD pathogenesis in the hippocampus and hypothalamus of the 5XFAD mouse model of amyloidosis, and explore the effect the metabolic regulators fructose, DHA, and NR on AD pathology and molecular pathways in individual cell populations.

## Methods

*Animals and conditions*

5XFAD mice were purchased from the Jackson Laboratory (MMRRC strain 34840). C57BL/6J mice were used as controls. There were five different conditions: (1) Control/wild-type (WT) with normal diet, (2) 5XFAD with normal diet, (3) 5XFAD fed high fructose diet (15% fructose w/v in drinking water), (4) 5XFAD fed high fructose diet and DHA (1.2% w/w; Nordic Naturals, Inc., Watsonville, CA, USA), and (5) 5XFAD fed high fructose diet and NR (3.6 g/kg of food; ChromaDex, Los Angeles, CA, USA). Dietary treatment started at month 2 of age and lasted for 3 months. At 1, 2, 3, 4, and 5 months of age, intraperitoneal glucose tolerance test (IPGTT) was carried out, and at 1, 2, and 3 months post-treatment learning and memory phenotypes were measured using Barnes maze test. AD pathology including Aβ (immunofluorescence) and phosphorylated tau (western blot) were measured.

*Single-cell RNA-sequencing (scRNAseq)*

There were 3 samples per group in hippocampus with a total of 15 samples. There were 3 samples per group for hypothalamus except for 5XFAD with normal diet which had 4 samples for a total of 16 samples. Papain was used to digest freshly dissected hippocampus and hypothalamus tissue. The cells were suspended using the protocol described in Brewer et al. [149] to a final concentration of 1000 cells/μl in 0.04% BSA-PBS. scRNAseq was conducted using the 10x Genomics platform (10x 3' single cell RNAseq V3 kit) at the UCLA Technology Center for Genomics & Bioinformatics (TCGB). Samples were then sequenced on the Novaseq S2 using 2x50bp setting at ~50k read/cell coverage.

*10X Genomics data pre-processing and quality control*

Reads were aligned to the mm10 genome and gene counts were calculated using CellRanger software (v 3.0.2) (10X Genomics). Filtered feature-barcode matrices from each library were loaded into Seurat (v 3.1.0) [https://github.com/satijalab/Seurat] and combined to create five different pooled digital gene expression matrices for wild-type, 5XFAD, 5XFAD with high fructose (5XFAD+F), 5XFAD with high fructose and DHA (5XFAD+F+DHA), and 5XFAD with high fructose and NR (5XFAD+F+NR). Single cells were selected based on a threshold of at least 100 genes and 500 transcripts and less than 20,000 transcripts and 15% mitochondrial gene expression. Transcript counts of each cell was normalized by the total expression for that cell, and the values were multiplied by 10,000 and log transformed (LogNormalize).

*Cell clustering and annotation*

Using Seurat, cells were projected onto two dimensions using T-distributed Stochastic Neighbor Embedding/ Uniform Manifold Approximation and Projection (t-SNE/UMAP) and assigned into clusters using Louvain clustering. Cell cluster specific marker genes consistent

across all samples were determined using FindConservedMarkers which employs a non-parametric Wilcoxon rank sum test that is run within each sample and calculates a meta p-value across all samples to assess the significance of each gene to be specific to each cluster. For each sample, the analysis is run between all cells of the cluster and all other cells. Genes tested must be expressed in at least 10% of the single cells in one group. These markers were manually evaluated for convergence on known cell type marker genes and used to label cell types.

*Quantitative assessment of global transcriptome shifts*

For each cell type, we generated a representative cell for the 5XFAD group and another for WT by calculating the average gene expression of all genes for each group within that cell type. We then calculate the Euclidean distance in gene expression between these representative cells to quantify the effect of 5XFAD on each cell type. To determine the significance of the observed Euclidean distance between 5XFAD and wild-type cells within each cell type, we estimated a null distribution by calculating the Euclidean distance between randomly sampled cells of the given cell type from both groups. This permutation approach is repeated for a total of 1000 times to generate the null distribution, which is compared to the Euclidean distance generated from the true 5XFAD and wild-type groups to determine an empirical p value. To correct for multiple testing across all the cell types tested, we calculated adjusted p-values using Bonferroni correction.

*Cell-cell interaction analysis*

We assessed cell–cell gene co-expression based on gene-level correlation patterns between two different cell types. To infer directionality of the interactions between the cell types, we designated the cell type whose marker genes encode secreted peptides from Uniprot as the source cell type and then correlated the expression of the secreted peptide-encoding genes

from the source cell type with genes in the target cell type. To deal with the sparsity of single cell data, we averaged the gene expression of WT and 5XFAD samples for each cell type. An interaction score is calculated from the sum of the correlation p-values for each peptide, assuming that a peptide from a source cell type with strong correlations with many genes in the target cell type would indicate strong interactions. To determine the significance of the interaction, we use a permutation approach in which a null distribution is drawn from the interactions scores generated by the correlations between source peptides and target genes where the expression values for each target gene has been shuffled independently.

*Differential gene expression (DEG) analysis and pathway enrichment*

The FindMarkers function from Seurat was used to compare gene expression between treatment groups to identify DEGs. The FindMarkers function is based on the same analysis as FindConservedMarkers (non-parametric Wilcoxon rank sum test). Genes tested must be expressed in at least 10% of the single cells in one group. Genes that passed an adjusted p-value threshold of 0.05 and a log fold change (logFC) threshold of 0.1 were used for pathway enrichment analysis with pathways from KEGG, BioCarta, Reactome, and hallmark genesets from the Molecular Signatures Database (MSigDB). Significant enrichment of pathways was based on a hypergeometric test followed by multiple testing correction with the Benjamini-Hochberg method. logFC of each pathway was calculated by summing all the individual pathway member gene logFC values.

*Cell lineage trajectory analysis*

Slingshot[128] was used to perform trajectory analysis on 5XFAD microglia in the UMAP space. Slingshot uses a cluster-based minimum spanning tree to construct the global lineage structure. It then fits smooth branching curves to the predicted lineages using simultaneous principal curves. We used a semi-supervised approach where only the starting cluster

(homeostatic cluster) was designated to guide the prediction. A generalized additive model was used to retrieve genes that changed as a function of pseudotime to capture both linear and non-linear patterns. The lineage with the greatest number of constituent clusters was analyzed.

*Test of DEGs for enrichment of human AD GWAS signals*

Marker set enrichment analysis (MSEA) from the Mergeomics pipeline[34] was used to perform AD GWAS enrichment of cell-type specific DEGs. DEGs with an FDR<0.05 and logFC>0.10 were used. Summary statistics from four large-scale AD GWAS in predominantly European populations were used[40,41,129,130]. The GWAS data was filtered for linkage disequilibrium. From GTEx version 8[42], hippocampus eQTLs and hypothalamic eQTLs were used to map GWAS loci to genes. The mapped genes were matched with the tissue-specific differentially expressed genes. Significance values from MSEA were adjusted to estimate the false discovery rate (FDR) using the Benjamini-Hochberg method.

*Drug repositioning using cell-type specific AD DEGs*

The Connectivity Map webserver from the Broad Institute was used for drug repositioning[131]. The tool used was 'Query'. Upregulated and downregulated differentially expressed genes with an FDR<0.05 and logFC>0.25 for each cell type were used as input where the max number of allowable genes was 150 each for upregulated and downregulated genes (300 max). 'Connectivity Scores' were retrieved from the analyses for plotting.

**Results**

*Metabolic and memory phenotypes*

The area under the curve (AUC) of the IPGTT test was elevated in only 5XFAD with regular diet at 8 weeks post-treatment (4 months of age), and at 12 weeks post-treatment (5

months of age), IPGTT AUC of 5XFAD with regular diet was similarly elevated to WT with fructose, known to cause metabolic syndrome[126], meaning that amyloidosis induced a systemic metabolic change. IPGTT AUC values at 12 weeks post-treatment were not elevated in 5XFAD with fructose, 5XFAD with fructose and DHA, and 5XFAD with fructose and NR. Starting at 9 weeks post treatment, 5XFAD with fructose, 5XFAD with fructose and DHA, and 5XFAD with fructose and NR had higher body weight than 5XFAD with regular diet. In the Barnes Maze test of memory, at 8 weeks and 12 weeks post-treatment, there was higher latency (longer time to recall) for 5XFAD with regular diet and 5XFAD with fructose which was comparable to the results of WT with fructose. NR and DHA improved memory in 5XFAD with fructose mice as the latency was shorter in these groups. These results were retrieved by personal communication from Lily Ying, Victoria Sánchez, and Fernando Gomez-Pinilla of the Gomez-Pinilla lab at UCLA.

*Cell-type classification from mouse wild-type and 5XFAD from the hippocampus and hypothalamus*

A total of 37,892 and 62,803 cells were profiled using 10x Genomics 3' Chromium scRNAseq platform in hippocampus and hypothalamus, respectively. All major cell types in hippocampus and hypothalamus were recovered using scRNAseq (**Figure 4**). Tanycytes were unique to hypothalamus, and choroid plexus cells were observed only in the hippocampus. Microgliosis and astrogliosis was evident in the 5XFAD condition as numbers of these cell types were significantly elevated compared to WT samples. A distinct cluster (Unknown 1) from a single WT sample in the hypothalamus highly expressed *Ttr* and shared some of the same markers as neurons and astrocytes. This effect was not observed for the same sample in the hippocampus.

The Euclidean distance between WT and 5XFAD cells provides a global measurement of transcriptional shifts and was used to rank cell-type sensitivity to the 5XFAD status (**Figure**

**4**). Based on this analysis, microglia and astrocytes were most affected by the 5XFAD condition in the hippocampus whereas oligodendrocytes and neurons were most affected in the hypothalamus.

*Genes and pathways disrupted by the 5XFAD status across cell types*

In many cell types in both the hippocampus and hypothalamus, the 5XFAD state was consistently accompanied with increased expression of genes involved in lipid transport, proteolytic, complement, and microglial activation including *Tyrobp*, *Trem2*, *Hexb*, and *Apoe*, and those encoding cathepsins and chemokines (**Figure 5**). While the majority of differentially expressed genes (DEGs) were upregulated, there were specific groups of genes that were downregulated, such as heat shock protein genes (*Hspa1a*, *Dnajb1*, *Hsp90aa1*, *Hsp90ab1*, *Hspa8*), splicing genes such as *Snrnp70*, and long non-coding RNA *Malat1*.

At the pathway level, immune system, lysosome, apoptosis, IL6 JAK STAT3 signaling, and K-Ras signaling were consistently upregulated across cell types in the hippocampus (**Figure 5**). Interestingly, in the hypothalamus, there was more downregulation of pathways and differential responses between cell types such as in the immune system pathway, which is strongly downregulated in microglia, endothelium2, oligodendrocytes, endothelium1, oligodendrocyte progenitor cells 1 (OPC1) and tanycytes, but is upregulated in oligodendrocyte progenitor cells 2 (OPC2), vascular smooth muscle cells, and minimally upregulated in astrocytes. In both the hippocampus and hypothalamus, TNFα signaling via NFκB was strongly downregulated in microglia. However, downregulation of immune system and interferon gamma response in the hypothalamus was not replicated in the hippocampus. In addition, hippocampal astrocytes strongly downregulated oxidative phosphorylation (OXPHOS) genes, whereas hypothalamic astrocytes exhibited a slight downregulation of these genes, and this pattern was the opposite for cholesterol homeostasis genes in that these were more strongly downregulated

in hypothalamic astrocytes than in hippocampal astrocytes. These examples provide evidence that cell type responses were specific to brain regions.

In a recent study analyzing both mouse and human single nuclei from the cortex[132], iron homeostasis alterations were found in human AD patients, but these changes were not significant in the 5XFAD mice that they analyzed. In our study, we see robust upregulation of *Ftl1* (ferritin light chain 1) and *Fth1* (ferritin heavy chain 1) across many cell types in both the hippocampus and hypothalamus. *Ftl1* and *Fth1* store iron in a non-toxic form. *Trf*, which encodes serotransferrin, a blood plasma glycoprotein that transports iron into the cell for storage, was also upregulated in hippocampal astrocytes, microglia, and OPC1. This upregulation may be in response to overexpression of the transgene *APP* (encoding amyloid precursor protein) as APP plays a role in iron homeostasis[133] and could be a neuroprotective mechanism as free iron is toxic in the brain[76]. However, *Trf* was downregulated in hypothalamic oligodendrocytes.

*Cell-type and tissue specific DEGs in 5XFAD*

First, we describe cell type specific but not tissue specific DEGs, meaning the cell-type specific DEG was shared between the hippocampus and hypothalamus (**Figure 6**). There were large numbers of these for the microglia only, which had 123 cell type specific DEGs shared between hippocampus and hypothalamus. In microglia, *P2ry12*, a homeostatic gene, was downregulated, and *Lpl*, an activated microglia gene was upregulated. Expectedly, these hallmark features of microglia are shared between hippocampus and hypothalamus. Other shared DEGs include the upregulation of *Sgk* and downregulation of *Polr3e* and *Sec11c* in oligodendrocytes, and the downregulation of *Camk2f*, *Mical2*, and *Acss2* in astrocytes. These sets of DEGs represent shared cell type mechanisms between the two tissues.

Second, we describe DEGs that were both cell type and tissue specific (**Figure 6**) wherein there were 14 and 5, 6 and 6, 32 and 80, 3 and 127, 2 and 32, for hippocampus and

hypothalamus, respectively, in astrocyte, ependyma, microglia, neuron, and pericyte populations. Among these include decreased expression of *Vgf* and *Syp* in hypothalamic neurons, decreased expression in *Kcna1* and *Slc20a2* in hypothalamic oligodendrocytes, and increased expression of *Scgb3a1* and *Hrct1* in hippocampal endothelium1 cells. Although these are considered tissue specific DEGs, there is a nonsignificant change usually in the same direction in the corresponding cell type of the other tissue, suggesting these genes are indeed more cell type specific than tissue specific.

We found a total of 328 choroid plexus cells from WT and 5XFAD mice. Choroid plexus epithelial cells act as a barrier between the blood and cerebrospinal fluid, produce cerebrospinal fluid, and serve as an entry point for substances and immune cells into the brain. There were 62 DEGs specific to choroid plexus which included reported AD GWAS genes such as *Sorl1*, *Slc14a2*, and *Hrk* which were upregulated in 5XFAD. *Aqp4*, encoding aquaporin 4, was specifically upregulated in choroid plexus cells in 5XFAD mice, and *Aqp4* upregulation and localization at the parenchymal processes of astrocytes of the cerebral cortex in 5XFAD mice has been shown to promote Aβ clearance[109]. While we did not see this upregulation in astrocytes, we did observe that choroid plexus cells and astrocyte shared differential gene expression changes such as the downregulation of OXPHOS genes and downregulation of *Col9a3* which was unique to these cell types. Other unique DEGs include *Nkain4* and *Tmem47*, though these were downregulated in astrocytes and upregulated in choroid plexus cells.

*Top hippocampus-specific and hypothalamus-specific genes*

Of all the 2093 unique DEGs, 818 were shared between hippocampus and hypothalamus, 576 were specific to the hippocampus, and 699 were specific to the hypothalamus. **Figure 7** shows five of these genes from each tissue. One hippocampus specific DEG is *C4b* which is upregulated in 5XFAD and has been shown to be increased in serum of AD patients[134]. *Avp* (vasopressin) is upregulated only in hypothalamus across many cell types

and vasopressin has been shown to be decreased in the suprachiasmatic nucleus of the hypothalamus in postmortem AD[115]. In a rat model of chronic cerebral hypoperfusion, vasopressin has been shown to improve spatial learning possibly by promoting synaptic plasticity[135]. Thus, this increase in *Avp* expression may be a compensatory response to degenerating neurons and neuronal processes which is defective in late-stage AD.

*Unique DEG patterns in microglia and astrocytes in 5XFAD*

Interestingly, gene expression changes in microglia and astrocytes were opposite to those of other cell types for certain DEGs (**Figure 8**). Microglia exhibited a distinct downregulation of several genes including *Junb*, *Ubc*, *Nfkbia*, *Tnf*, *Sgk1*, *Fos*, *Nfkbiz*, *Zfp36*, *Jun*, *Egr1*, *Atf3*, *Fosb*, *Ptgds*, *Ier3*, *Socs3*, *Csf1r*, and *Ier2* and downregulation of pathways including TNFα signaling via NFκB and p53 pathway, which were largely upregulated in other cell types. Astrocytes exhibited a distinct downregulation of *Fabp5*, *Ptprz*, and *Gapdh* which were upregulated in other cell types. In addition, OXPHOS genes were significantly downregulated in astrocytes and choroid plexus cells but upregulated in all other cell types of the hippocampus. As described in Zhou et al. for human AD, the downregulation of *Fabp5* in astrocytes was indicative of decreased coordination between astrocytes and neurons[132]. Indeed, this is also exemplified in our cell-cell communication network analysis where there was a loss of astrocytic communication with neurons, whereas astrocytic communication with other cell types was increased (**Figure 9**). This loss of communication was inferred from decreased astrocyte secreted peptide coexpression with neuronal genes.

*Human AD GWAS enrichment of 5XFAD cell type specific differentially expressed genes*

We integrated human GWAS of AD with DEGs from each cell type using marker set enrichment analysis (MSEA) from the Mergeomics pipeline[34] (**Figure 10**). We used summary statistics for the Jun et al., UK Biobank, Kunkle et al., and Jansen et al. AD GWAS

studies[40,41,129,130] and hippocampus eQTLs and hypothalamus eQTLs from GTEx[42] to map loci to genes. We found hippocampal microglial DEGs to be highly enriched for AD GWAS signals across all 4 AD GWAS studies. The genes mapped from AD GWAS loci that overlapped with microglia DEGs included *APOC4*, *HLA-DQB1*, *TRIM47*, *CTSB*, *ALDH2*, and *PTGS1*. Oligodendrocyte, OPC1, and astrocyte DEGs were significantly enriched for GWAS signals from the Jun et al. and Kunkle et al. studies only.

There was no significant enrichment of AD GWAS signals with DEGs from hypothalamic DEGs even though the DEG numbers were comparable to that of hippocampus and number of eQTLs were also similar to hippocampus (data not shown). Interestingly, this may mean that the strongly associated risk loci for AD map significantly more to genes that are uniquely altered in hippocampus.

*Microglial 5XFAD subpopulations and trajectory inference of activation events*

In microglia of the hippocampus, we identified previously described homeostatic clusters and activated or disease-associated microglia (DAM) using canonical homeostatic and reactive microglia genes[136]. Activated microglia were exclusive to 5XFAD samples. We also observed considerable heterogeneity in activated microglia. We performed pseudotime analysis using Slingshot[128] and found genes that increase in expression along a trajectory from homeostatic to DAM (**Figure 11**). We group the top 500 genes that changed as a function of pseudotime into 15 pseudotime groups that have differential changes in gene expression along the constructed pseudotime and performed pathway enrichment on these groups for functional annotation (**Figure 11**). Genes from group 10 are homeostatic genes and are enriched for chemokine signaling. Genes from group 13 are specifically enriched in pyruvate metabolism genes and are highly expressed in the transition phase from homeostatic microglia to late-stage DAM. Late-stage DAM microglia, the terminal cluster, highly expressed genes from group 1 which were enriched for lysosomal genes.

We also find novel homeostatic markers such as *Herpud1*, *Glul*, *Kctd12*, *Pld4*, *Ltc4s*, *Alox5ap*, *Camk2n1*, and *Crybb1*. Expectedly, there was no overlap between DAM marker genes from the Keren-Shaul et al. study and genes in our pseudotime group 10 (homeostatic markers). Of the 88 DAM genes, 49 were captured in our top 500 pseudotime genes across 8 groups with most overlapping with pseudotime group 1. Novel DAM markers identified in our study include *Il4i1*, *Pdcd1*, *Egr2*, *Plau*, *Ldlr*, and *Msmo1*.

The marker genes of the terminal cluster predicted by the pseudotime analysis was the only cluster that was significantly enriched in mapped genes from AD GWAS loci such as *APOC4*, *HLA*- genes, *ALDH2*, *CD52*, *CTSH*, *ANXA5*, *TIMP2*, *CTSZ*, and *GPNMB*, which are the same ones in the main microglia cluster DEGs which showed AD GWAS enrichment (**Figure 10**). This confirms the pseudotime position of the terminal cluster as “fully activated” microglia as the genes in this cluster are most strongly associated with AD in human GWAS.

*Neuronal sub-population specific differential gene expression*

A total of 10,023 neurons from the hypothalamus and 1,205 from the hippocampus were identified (**Figure 12**). All major hippocampal neurons were recovered including CA1, CA3, inhibitory interneurons, subiculum, entorhinal, and dentate gyrus. For a few of these major classes, subtypes were identified and named with their unique marker gene. In the subiculum population, two populations were identified with marker genes *Dkkl1* and *Coro6*; in the GABAergic interneurons, *Six3* and *Crhbp* expressing sub-clusters were identified; in entorhinal neurons, *Ccer2* and *Ly6g* expressing sub-clusters were identified. We observed the greatest shift in transcriptional profiles by 5XFAD status in the Cajal Retzius neurons.

The neuronal subtype DEGs between 5XFAD and WT were similar with those of the overall clustering including increases in *Apoe*, *Tyrobp*, *C1qa*, *C1qb*, *Cst3*, *Ctsd*, *Ccl4*, and *Fth1* expression. A DEG specific to CA1 Subtype 1 (CA1 neurons highly expressing *Cpne7*), Reticulon 3 (*Rtn3*), which may be involved in membrane trafficking and inhibits beta-amyloid

converting enzyme activity[137], was downregulated 2.3-fold and was not a DEG for the main neuronal DEG analysis, but was downregulated in hypothalamic oligodendrocytes in the main cluster 1.2-fold. Considering its inhibition of Aβ production, its downregulation would exacerbate Aβ accumulation and may be indicative of degenerating neurons in 5XFAD mice. Other reticulons also act to inhibit Aβ production; *Rtn1* was upregulated in hypothalamic astrocytes, endothelium cells, oligodendrocytes, pericytes, and the vascular smooth muscle cells, but not differentially regulated in the hippocampus. *Rtn4* was downregulated in oligodendrocytes of both the hippocampus and hypothalamus. Our data show differential region specific and cell type specific reticulon responses, and further investigation of their functions is needed.

For hypothalamic neuronal sub-clustering, the major subtypes were identified by their high specific expressions of secreted neuropeptides including *Pomc*, *Vip*, *Vtn*, *Agrp*, *Nrgn*, *Tac2*, and *Oxt*. The *Tac2* (tachykinin 2) and *Oxt* (oxytocin/neurophysin I prepropeptide) expressing clusters were dominated by 5XFAD cells (Tac2: 73 to 7; Oxt: 52 to 6, 5XFAD to WT cells, respectively). Tachykinin 2 has been shown to induce behavioral changes such as aggression and sensitivity in chronic social isolation stress[138]. Therefore, because we see an increase in *Tac2* expressing neurons in response to amyloidosis, molecular stress may cause similar effects to those of affective chronic stress. This effect may explain in part the increased aggression that was observed in the 5XFAD mice and the mood and behavioral changes seen in AD[139]. In addition, the increase in *Oxt* expressing neurons is in agreement with findings that oxytocin levels are increased in AD patients[140].

*Comparison of differentially expressed genes in human AD single-cell studies*

We compared our cell-type specific DEGs to those of the Mathys et al. single-nucleus RNA-seq (snRNAseq) study on prefrontal cortex of human AD patients[141]. They performed differential gene expression analysis on both late-pathology versus early-pathology and pathology versus no pathology. We draw our comparisons to the pathology versus no pathology

DEG analysis. We acknowledge the difference in brain regions and hope to compare pan-regional responses such as those we see shared in both hippocampus and hypothalamus.

Of the shared DEGs, many were oppositely regulated between 5XFAD and human AD conditions. In the comparison between DEGs of human excitatory neurons and mouse hippocampal neurons, 94 of the 126 shared genes were oppositely regulated, many of which were ribosomal genes (*Rpl*-, *Rps*-). Likewise, 106 out of 189 shared genes between oligodendrocytes of human prefrontal cortex and of mouse hippocampus were oppositely regulated. There was a similar comparison with DEGs of the hypothalamus, in that most neuronal and oligodendrocyte genes shared between human AD and mouse 5XFAD had opposite directions in the studies. For astrocytes in both hippocampus and hypothalamus, more differentially expressed genes had the same direction, and for microglia in both hippocampus and hypothalamus, the numbers of DEGs with shared direction versus DEGs with opposite directions were near equal. This may be due to differential timings of alterations across different cell types. For example, in considering the human post-mortem samples as late-stage AD, 5XFAD astrocytes may exhibit a diseased state early in Aβ accumulation and thus have gene expression changes similar to that of late-stage AD astrocytes. For other cell types with more discordant gene changes between human AD and mouse 5XFAD, the gene expression changes may represent compensatory mechanisms that are impaired in human AD, possibly contributing to or accelerating AD pathogenesis, or may represent regional differences between the prefrontal cortex, hippocampus, and hypothalamus.

Among the shared genes with the same differential change in human AD and mouse 5XFAD were *Apoe* (*APOE*, apolipoprotein E, upregulated) in neurons and microglia, neuronal *Igf1* (*IGF1*, insulin growth factor, downregulated), neuronal and oligodendrocyte *Clu* (*CLU*, clusterin, upregulated), and *Gfap* (*GFAP*, glial fibrillary acidic protein, upregulated) in neurons, oligodendrocytes, and astrocytes. These gene expression changes likely represent cellular mechanisms to combat Aβ deposition. Among those that had opposite changes were *Fth1*

(*FTH1*, ferritin heavy chain) which was downregulated in human AD cortex neurons and astrocytes but upregulated in 5XFAD across many different hippocampal and hypothalamic cell types, *Sparcl1* (*SPARCL1*, secreted protein acidic and rich in cysteine like) which was downregulated in human AD and upregulated in 5XFAD hippocampal oligodendrocytes and hypothalamic neurons, oligodendrocytes, and microglia, and *Gprc5b* (*GPRC5B*, G-protein coupled receptor) which was upregulated in human AD and downregulated in 5XFAD hippocampal astrocytes and oligodendrocytes and hypothalamic oligodendrocytes. *Sparcl1* is involved in synaptic maintenance, and single nucleotide polymorphisms (SNPs) leading to lower expression of *SPARCL1* in humans is associated with accelerated memory loss and brain atrophy[142]. *GPRC5B* is hypothesized to reduce insulin secretion and also mediate neuronal differentiation[143,144]. The downregulation of *FTH1* in human AD may exacerbate neurotoxicity, given its role in iron homeostasis as discussed previously, but the upregulation of *Fth1* and *Ftl1* in 5XFAD mice may represent an intact neuroprotective mechanism.

*Reversal of 5XFAD transcriptional signatures by fructose*

We fed 5XFAD mice with a high fructose diet and compared their gene expression profiles with those of normal diet 5XFAD mice. We observed consistent and robust reversal of 5XFAD transcriptional signatures across many different pathways (**Figure 13**). The 5XFAD regulation of oxidative phosphorylation (OXPHOS), adipogenesis, xenobiotic metabolism, complement, and TNFα signaling via NFκB pathways was consistently reversed by fructose across cell types. Fructose induced a downregulation of OXPHOS across all major cell types except astrocytes. Neurons showed a modest upregulation of OXPHOS in 5XFAD and a strong downregulation of OXPHOS in 5XFAD with fructose. The increased supply of energy from fructose may lead to a homeostatic response to decrease energy production or may lead to a detrimental impairment of OXPHOS gene expression. Immune system genes were further upregulated in 5XFAD with fructose in microglia, oligodendrocyte, endothelial, and OPC1,

whereas it was upregulated in 5XFAD and downregulated in 5XFAD with fructose for neurons and pericytes.

Interestingly, there was a consistent decrease in gene expression across many different pathways for hippocampal neurons. **Figure 14** shows additional pathways downregulated by fructose in hippocampus neurons compared to hypothalamic neurons. For most pathways, neurons are not significantly affected by the 5XFAD status. In an already stressed state of amyloidosis, fructose may instigate cellular insult to neurons, leading to a robust downregulation of various pathways. For example, the 5XFAD status does not affect mitochondrial protein import in hippocampal neurons, but with high fructose diet, these genes are robustly downregulated. Mitochondrial protein import is important for proteostasis; proteases in mitochondria eliminate misfolded and damaged proteins. A downregulation of this pathway would exacerbate the Aβ accumulation. Likewise, genes relating to proteasome, a complex that contains proteases, are downregulated, also possibly leading to an exacerbation of Aβ aggregation. Hypothalamic neurons show markedly different responses from hippocampal neurons. Hypothalamic neurons are much more sensitive to the 5XFAD status, as recapitulated in the Euclidean distance analysis (**Figure 4**). Unfolded protein response, glycolysis, and membrane trafficking is downregulated by fructose in hypothalamic neurons which is opposite to the effect in hippocampal neurons. Pathways that were similar between hippocampal and hypothalamic neurons include mRNA splicing and transcription, which were downregulated.

*Effects of DHA and NR on the fructose-induced alterations of the 5XFAD transcriptional signatures*

To investigate nutritional alterations in well-known AD genes, in **Figure 15**, we examine the effect of fructose, DHA, and NR on three GWAS genes in the hippocampus. *APOE*, *CLU*, and *TREM2* are upregulated in human AD such as in the previously described Mathys et al. snRNAseq study[141] and are hypothesized to have important functions in Aβ clearance. *Apoe*,

*Clu*, and *Trem2* are similarly upregulated in the 5XFAD condition. This was reversed by fructose, representing either an impairment in the necessary mechanisms for Aβ plaque clearance or an indication that there is no longer a cellular stress response due to less Aβ deposition, though high fat diet, which also induces metabolic syndrome, in an AD mouse model was shown to decrease Aβ clearance[23], but high fructose diet may produce a different effect. NR marginally increased *Apoe* expression in endothelial cells and neurons and *Clu* expression in endothelial, microglial, oligodendrocyte, and pericyte cells. DHA modestly increased *Apoe* expression in endothelial cells. There were no large regulations of *Trem2* by any dietary interventions, though DHA further decreased *Trem2* expression in astrocytes with a minor fold change.

In **Figure 16**, we plot the top 30 DEGs regulated by 5XFAD for astrocytes and oligodendrocytes and observe very consistent reversal of the 5XFAD signature by fructose. We represent both the effect of DHA or NR in the 5XFAD with fructose condition and the effect of DHA+fructose or NR+fructose (effect of both nutritional interventions) in the 5XFAD condition (labeled as DHA+Fructose on AD or fructose+DHA on AD). These comparisons also showed that fructose has a strong regulatory effect. In contrast, the individual contributions of DHA and NR are subtle and likely masked by fructose. Interestingly, while there was little effect of DHA and NR in the 5XFAD with fructose condition for most genes, *Ftl1* expression was robustly increased by DHA and NR in the 5XFAD with fructose condition. We also see the same pattern for *Fth1*, albeit modest compared to that of *Ftl1*. As we predict these genes are neuroprotective by promoting the storage of potentially detrimental free iron, we hypothesize this change to be beneficial in the stressed state of amyloidosis. The effect of DHA and NR causing gene expression changes to shift back to the 5XFAD state is also seen in *Aldoc* and *Gfap* for hypothalamic microglia and in *Ccl4* for hippocampal astrocytes. In hippocampal microglia, NR reverses fructose-induced downregulation of *Gfap*. In contrast, DHA/NR further enhances the fructose enhancement of the 5XFAD effect of *Cd9* and *Fcer1g* upregulation. These diverse

effects demonstrate the differential gene-specific responses to these nutritional interventions. Because many of these top DEGs are microglia activation genes, we speculate that fructose impairs microglia activation. Although overactive microglia can lead to deleterious neuroinflammation and neuronal pruning[145], the function of DAM to phagocytose and clear Aβ plaques is crucial to maintaining Aβ balance in the brain[146]. Therefore, the reversal effect of fructose may be detrimental in this regard.

With the inability to observe the DHA and NR effect in isolation on the 5XFAD background, we sought to see pathway changes seen in the comparison 5XFAD+DHA+fructose versus 5XFAD that was not observed in 5XFAD+fructose versus 5XFAD, and likewise for NR. In this way, we hope to identify a "quasi" DHA and NR effect in isolation. We saw significant "quasi" DHA and NR effects in astrocytes and choroid plexus cells of the hippocampus (**Figure 17**). In astrocytes, we see a robust upregulation of mitochondrial protein import genes by 5xFAD+DHA+fructose versus 5XFAD background which was not seen in the comparison of 5XFAD+fructose versus 5XFAD. We therefore suspect that DHA was the causal factor in upregulating mitochondrial protein import genes. We hypothesize this increase in expression of mitochondrial protein import genes by DHA would alleviate Aβ aggregation. In choroid plexus cells, NR downregulated immune system, cell cycle, cholesterol homeostasis, complement, and apoptosis pathways which were largely unaffected by fructose alone. We may speculate the effects of solely DHA and NR in these comparisons, but interactions between DHA and fructose and NR and fructose could also contribute to the observed effects.

*Connectivity map drug repositioning on cell type specific differentially expressed genes*

We performed Connectivity Map drug repositioning[131] using cell-type specific 5XFAD differentially expressed genes. In **Figure 17**, we plot the 'Connectivity Score' as the fill color in the heat map. This score is calculated based on a nominal p-value using the Kolmogorov-Smirnov enrichment statistic that is based on comparing the similarity between the query and

the reference signature to a null distribution of random queries. Another component of the score is ‘tau’ which compares the observed enrichment score to all other reference signatures in the database. For example, a ‘tau’ of 90 means just 10% of reference drug signatures show a stronger connectivity to the query. A strong positive score shown as greener in the heat map (**Figure 17**) means the input query and the drug reference signature has a similar differential gene expression profile. A strong negative score shown as more purple means the genes of the input query and the drug reference signature highly overlap, but the gene expression changes are opposite. The predicted drug velnacrine served as a positive control for the drug repositioning approach as it is a cholinesterase inhibitor belonging to a class of compounds that is already used in treatment of AD[102]. Its gene signature was negatively correlated to the 5XFAD signature across many cell types, meaning it can normalize the 5XFAD signature. We also found BX-795 to be highly similar to the DEGs in 5XFAD across many cell types, and phensuximide to be highly in opposition to the DEGs in 5XFAD across many cell types. Phensuximide is an anticonvulsant in the succinimide class and affects the expression of complement and serine peptidase genes. This is consistent with our observations of upregulation of proteolysis and complement genes in the 5XFAD signature across many cell types. BX-795 is a 3-Phosphoinositide-dependent protein kinase 1 inhibitor that inhibits HSV-1 and HSV-2 replication.

**Discussion**

We have comprehensively characterized the cell type specific and tissue specific transcriptional alterations in the 5XFAD model for AD and have observed drastic changes to these responses by high fructose diet. Although fructose reversed many 5XFAD transcriptional signatures, we hypothesize that fructose may indeed exacerbate AD pathology by impairing particular neuroprotective mechanisms such as the storage of iron in a non-toxic form, impairing

microglial function, and downregulating many neuronal processes such as proteostasis. DHA and NR had effects on expression levels of select genes such as *Ftl1* and *Fth1* which reversed the fructose-induced downregulation of these iron storing genes, effectively restoring this particular mechanism of iron homeostasis. Thus, metabolic syndrome may exacerbate AD pathology by counteracting Aβ clearance mechanisms and compensatory responses to cellular stress, and nutritional supplementation of DHA and NR may have certain benefits to enhance Aβ clearance and promote the cellular responses to maintain neuronal and glial fitness. However, our condition of these metabolic modulators on the background of high fructose diet may have obscured some of their effects since the regulatory effects of fructose was extremely robust. Additional experiments are being carried out to examine the effects of DHA and NR in the absence of fructose treatment.

While we recovered large numbers of glial cells and have thoroughly resolved activated microglia subtypes and plan to investigate other important pathogenic players such as astrocytes, oligodendrocytes, and endothelial cells, we were not able to recover many neurons and did not have sufficient numbers of neuronal subtypes for meaningful and well-powered analysis. However, we tout our recovery of choroid plexus cells and robust choroid plexus-specific gene expression changes, which, to our knowledge, has not been explored in the single cell context of AD.

As there is growing evidence that AD pathogenesis may be driven by systemic metabolic changes, we acknowledge the utility of investigating other tissues besides the brain which will open new avenues of research into cross-talks between peripheral tissues and the brain.

While we seek to understand AD in its entirety, we acknowledge the lack of concordance between the 5XFAD model and the most common form of AD, late-onset AD (LOAD), especially in its pathogenesis. The 5XFAD model is based on familial mutations in AD, whereas LOAD is due to both genetic factors and environmental influences. In addition, tau aggregations are another defining feature of AD which is absent in the 5XFAD model. Despite these limitations,

5XFAD has been used as an important AD model to characterize the cellular responses to Aβ accumulation, and by drawing comparisons to other AD models and LOAD, we can understand the similarities and differences.

Finally, we predict many drugs that regulate 5XFAD signatures in both a cell type specific manner and across many different cell types and may be useful in the prevention or reversal of AD. As discussed previously that the 5XFAD signature may represent both compensatory and deleterious responses, careful consideration of drug prioritization to produce the desired result is needed. Also, the heterogeneity in drug predictions across different cell types also emphasizes the need to evaluate all possible cell-type specific effects of a drug which will inform on combination therapies.

## Tables

**Table 1. Bayesian network resources.**
Datasets from several studies were used to construct bayesian networks used in the analysis. The references and descriptions for the datasets are listed in the chart below.

| Tissue | Species | Dataset descriptions | References |
|---|---|---|---|
| Adipose tissue | Human | 1,675 individuals from two Icelandic cohorts | Emilsson, 2008[147] |
| | Mouse | C57BL/6J x A/J mouse cross | Derry, 2010[148] |
| | Mouse | C57BL/6J x C3H ApoE -/- mouse cross | Wang, 2007[149] |
| | Mouse | C57BL/6J x C3H wildtype mouse cross | Schadt, 2008[150] |
| | Mouse | C57BL/6J x BTBR Lepob mouse cross | Tu, 2012[151] |
| Blood | Human | 1,675 individuals from two Icelandic cohorts | Emilsson, 2008 |
| Brain | Mouse | C57BL/6J x A/J mouse cross | Derry, 2010 |
| | Mouse | C57BL/6J x C3H ApoE -/- mouse cross | Wang, 2007 Yang, 2006[152] |
| | Mouse | C57BL/6J x BTBR Lepob mouse cross | Tu, 2012 |
| | Human | 57 subjects ranging from 5.7 weeks post-conception to 82 years; samples taken from 16 regions and from both hemispheres; 1,340 samples total | Kang, 2011[153] |
| Liver | Human | 427 individuals | Schadt, 2008 |
| | Mouse | C57BL/6J x A/J mouse cross | Derry, 2010 |
| | Mouse | C57BL/6J x C3H ApoE -/- mouse cross | Wang, 2007 Yang, 2006 |
| | Mouse | C57BL/6J x C3H wildtype mouse cross | Schadt, 2008 |
| | Mouse | C57BL/6J x BTBR Lepob mouse cross | Tu, 2012 |
| Muscle | Mouse | C57BL/6J x A/J mouse cross | Derry, 2010 |
| | Mouse | C57BL/6J x C3H ApoE -/- mouse cross | Wang, 2007 Yang, 2012 |
| | Mouse | C57BL/6J x C3H wildtype mouse cross | Tu, 2012 |
| | Mouse | C57BL/6J x BTBR Lepob mouse cross | Tu, 2012 |

**Information for Tables 2-4:**
SNP mapping method aliases: Numbered aliases of SNP to gene mapping methods are as follows (3-54 tissue mapping methods have ‘e’ and ‘s’ designations in the tables representing eQTL and sQTL, respectively): 1: Distance, 2: ENCODE, 3: All combined, 4: Peripheral combined, 5: Brain combined, 6: Adipose Subcutaneous, 7: Adipose Visceral Omentum, 8: Adrenal Gland, 9: Artery Aorta, 10: Artery Coronary, 11: Artery Tibial, 12: Brain Amygdala, 13: Brain Anterior cingulate cortex BA24, 14: Brain Caudate basal ganglia, 15: Brain Cerebellar Hemisphere, 16: Brain Cerebellum, 17: Brain Cortex, 18: Brain Frontal Cortex BA9, 19: Brain Hippocampus, 20: Brain Hypothalamus, 21: Brain Nucleus accumbens basal ganglia, 22: Brain Putamen basal ganglia, 23: Brain Spinal cord cervical c-1, 24: Brain Substantia nigra, 25: Breast Mammary Tissue, 26: Cells Cultured fibroblasts, 27: Cells EBV-transformed lymphocytes, 28: Colon Sigmoid, 29: Colon Transverse, 30: Esophagus Gastroesophageal Junction, 31: Esophagus Mucosa, 32: Esophagus Muscularis, 33: Heart Atrial Appendage, 34: Heart Left Ventricle, 35: Kidney Cortex, 36: Liver, 37: Lung, 38: Minor Salivary Gland, 39: Muscle Skeletal, 40: Nerve Tibial, 41: Ovary, 42: Pancreas, 43: Pituitary, 44: Prostate, 45: Skin Not Sun Exposed Suprapubic, 46: Skin Sun Exposed Lower leg, 47: Small Intestine Terminal Ileum, 48: Spleen, 49: Stomach, 50: Testis, 51: Thyroid, 52: Uterus, 53: Vagina, 54: Whole Blood

**Table 2. Shared genetically informed canonical pathways between AD and T2D.**
Suggestive GWAS genes (p<0.001) in black are replicated across all four studies and those in gray are replicated in three studies for the particular mapping method (in at least one of them).

| Source | Pathway Description | Mapping | Ex. Suggestive Genes |
|---|---|---|---|
| Reactome | Adaptive Immune System | 1, 3e, 3s, 4e, 4s, 6e, 9e, 11e, 26e, 31e, 33e, 40e, 45e, 46e, 54e, 40s, 45s | MICA, MICB, TAP2, PSMC5 |
| Reactome | Class I MHC mediated antigen processing & presentation | 1, 2, 3s, 4e, 4s, 6e, 9e, 11e, 26e, 31e, 40e, 54e, 40s, 45s | TAP2, PSMB9, PSMC5 |
| GWAS Catalog | Positive control gene set for coronary heart disease | 1, 2, 3e, 3s, 4e, 5e, 17e, 21e, 39e, 40e | HCG27, HLA-C, SLC12A9, CDKN2A, CDKN2B, HLA-C, MTAP, TOMM40, BTNL2 |
| Reactome | Immune System | 3e, 4e, 4s, 26e, 33e, 40e, 45e, 46e, 45s | C2, C4B, CFB, KLC1, CD79B |
| GWAS Catalog | Positive control gene set for HDLC | 1, 2, 3e, 4e, 5e, 37e, 46e, 48e | PVRL2, TOMM40 |
| Reactome | Complement cascade | 2, 3e, 4e, 6e, 37e, 40e, 51e | C4A, C4B |
| Reactome | Triglyceride Biosynthesis | 3e, 3s, 4e, 4s, 6s | AGPAT1, ELOVL5, GPAM |
| Reactome | RIG-I/MDA5 mediated induction of IFN-alpha/beta pathways | 3e, 4e, 39e, 40e, 46e | AGER |
| KEGG | Glycerolipid metabolism | 3e, 3s, 4e, 4s, 40e | AGPAT1 |
| KEGG | Complement and coagulation cascades | 4e, 33e, 34e, 37e, 40e, 51e | C4A, C4B |
| Reactome | Metabolism of proteins | 1, 2, 3e, 4e | ACHE, RPL13, SKIV2L, ACE, B4GALT5, TOMM40 |
| Reactome | Toll-Like Receptors Cascades | 3e, 4e, 40e, 46e | AGER |
| Reactome | Integration of energy metabolism | 3e, 3s, 4e, 4s | AGPAT1 |
| Reactome | Fatty acid, triacylglycerol, and ketone body metabolism | 3e, 3s, 4e, 4s | AGPAT1 |
| Reactome | Cell Cycle | 2, 4e, 4s, 7e | CDKN2B, CDNK2B, PSMB9 |
| Reactome | TRAF6 mediated NF-kB activation | 3e, 4e, 40e, 46e | AGER |
| Reactome | Metabolism of lipids and lipoproteins | 3e, 4e, 4s | ACHE, AGPAT1, SLC44A4 |
| Reactome | Signaling by Insulin receptor | 3e, 4e, 40e | ATP6V1G2 |
| GWAS Catalog | Positive control gene set for TC | 1, 2, 3e, 4e | DHX38, HP, HPR, TOMM40 |
| Reactome | Advanced glycosylation endproduct receptor signaling | 3e, 4e | AGER |
| KEGG | Notch signaling pathway | 4e, 6e | NOTCH4 |
| BioCarta | Lectin Induced Complement Pathway | 3e, 4e | C4B, C2, MASP1 |
| Reactome | Gene Expression | 3e, 4e | EHMT2, NOTCH4, SF3B3 |
| GWAS Catalog | Positive control gene set for T2DM | 1, 2 | CDKN2A, CDKN2B, TCERG1L, HLA-DQA2 |
| Reactome | Regulation of Lipid Metabolism by Peroxisome proliferator-activated receptor alpha (PPARalpha) | 4e | FADS1, FDFT1, AGT, PPARG |
| Reactome | Transcriptional Regulation of White Adipocyte Differentiation | 4e | PPARG, FABP4, MED10 |
| Reactome | Phase 1 - Functionalization of compounds | 28e | CYP21A2 |
| KEGG | Spliceosome | 3e | DHX38, SNRPD2 |
| Reactome | Transferrin endocytosis and recycling | 40e | ATP6V1G2 |
| Reactome | Insulin receptor recycling | 40e | ATP6V1G2 |
| Reactome | HIV Infection | 4e | VPS28, GTF2H4, NELFE |
| Reactome | Endogenous sterols | 4e | CYP7A1, CYP17A1 |

## Table 3. AD-specific genetically informed pathways.

| Source | Pathway Description | Mapping | Ex. Suggestive Genes |
|---|---|---|---|
| Reactome | Immunoregulatory interactions between a Lymphoid and a non-Lymphoid cell | 1, 2, 3e, 3s, 4e, 4s, 11e, 26e, 33e, 37e, 39e, 46e | PVR, MICB |
| KEGG | Hematopoietic cell lineage | 3e, 4e, 4s, 5e, 8e, 28e, 32e, 37s, 40s, 54s | CD55, CD33, CR1 |
| Reactome | Protein folding | 2, 3e, 4e, 5e, 11e, 25e, 26e, 33e, 40e, 46e | SKIV2L, PFDN1 |
| KEGG | Oxidative phosphorylation | 3e, 4e, 5e, 11e, 26e, 40e, 42e, 46e, 48e, 51e | ATP6V1G2, COX11, NDUFA2 |
| KEGG | RNA degradation | 2, 3e, 4e, 5e, 11e, 26e, 33e, 40e, 46e | SKIV2L |
| Reactome | Retinoid metabolism and transport | 1, 2, 3e, 4e, 5e, 33e, 37e, 46e | APOC2, APOE, GPC2 |
| BioCarta | Endocytotic role of NDK, Phosphins and Dynamin | 1, 2, 3e, 3s, 4e, 4s, 32e, 45e | BIN1, PICALM |
| Reactome | Metabolism of RNA | 2, 3e, 3s, 4e, 4s, 7e, 47e, 45s | GEMIN7, PSMB8, RPL13 |
| KEGG | Alzheimer's disease | 1, 4e, 5e, 11e, 46e, 48e, 51e | APOE, APP, ADAM10 |
| Reactome | Lipid digestion, mobilization, and transport | 1, 2, 3e, 4e, 37e, 46e | APOE, APP |
| Reactome | Signaling by Wnt | 3e, 3s, 4e, 4s, 7e, 45s | PSMB9, MANEA |
| Reactome | Transmission across Chemical Synapses | 3e, 4e, 9e, 11e, 31e, 51e | ACHE, GABBR1, GNGT2 |
| Reactome | Phagosomal maturation (early endosomal stage) | 3e, 4e, 11e, 26e, 40e | ATP6V1G2, CYBA, NCF2 |
| KEGG | RNA polymerase | 1, 3e, 4e, 11e, 26e, 32e | POLR2E |
| Reactome | Binding and Uptake of Ligands by Scavenger Receptors | 1, 2, 4e, 37e, 45e, 46e | APOE, HPR, HP |
| Reactome | Neuronal System | 4e, 9e, 11e, 31e, 51e | STX1B, STX4, KCNN4 |
| Reactome | Clathrin derived vesicle budding | 1, 2, 3e, 4e, 26e | PICALM, STX4, BLOC1S3 |
| KEGG | Endocytosis | 2, 3e, 4e, 31e | CBLC, HSPA1B, USP8, HSPA1L |
| KEGG | Focal adhesion | 3e, 4e, 8e | ZYX, DOCK1, VAV3, TLN2 |
| KEGG | Pyrimidine metabolism | 3e, 26e, 28e, 32e | DHODH, ZNRD1, POLR2E |
| Reactome | ECM proteoglycans | 3e, 4e, 54e | ITGAX |
| Reactome | tRNA Aminoacylation | 2, 4s, 21e | VARS2, VARS |
| Reactome | Cytokine Signaling in Immune system | 3s, 4s, 45s | PTK2B, PSMB8 |
| Reactome | Meiosis | 5e, 22e | STAG3, MSH5 |
| Reactome | The citric acid (TCA) cycle and respiratory electron transport | 4e, 5e | NDUFS3, SDHB, PDPR, SLC16A8, PDK1, NNT |
| Reactome | Pyruvate metabolism and Citric Acid (TCA) cycle | 4e, 5e | SDHB, PDPR, SLC16A8, PDK1, NNT |
| Reactome | Mitochondrial Protein Import | 1, 2 | TOMM40 |
| Reactome | Cell-cell junction organization | 1, 2 | CDH4, PVR, PVRL2 |
| KEGG | Adherens junction | 1, 2 | PVRL2, TGFBR2, CSNK2B, BAIAP2 |
| Reactome | snRNP Assembly | 2, 39e | GEMIN7, SNRPB, SNRPD2 |
| Reactome | Meiotic Synapsis | 5e | STAG3 |
| Reactome | Meiotic Recombination | 5e | MSH5 |
| KEGG | NOD-like receptor signaling pathway | 3e | PYDC1, TRIP6 |
| KEGG | Amyotrophic lateral sclerosis (ALS) | 1 | BCL2, TOMM40 |
| KEGG | ErbB signaling pathway | 1 | CBLC, HBEGF, NRG1 |
| Reactome | mRNA Splicing - Minor Pathway | 1 | POLR2E, SNRPD2 |
| Reactome | Mitochondrial tRNA aminoacylation | 2 | VARS2 |
| KEGG | Tight junction | 2 | CSNK2B |

**Table 4. T2D-specific genetically informed pathways.**
Suggestive GWAS genes ($p < 0.001$) in black are replicated in at least two studies and those in gray are significant in one study.

| Source | Pathway Description | Mapping | Ex. Suggestive Genes |
|---|---|---|---|
| KEGG | PPAR signaling pathway | 1, 2, 3e, 4e, 33e | EHHADH, FABP4, FADS2, LPL, NR1H3, PPARG, SCD5, ACSL1 |
| GWAS Catalog | Positive control gene set for HbA1c | 1, 2, 3e, 4e | ANK1, CDKAL1, GCK, TCF7L2 |
| GWAS Catalog | Positive control gene set for BMI | 1, 2, 3e, 4e | CDKAL1, FTO, GIPR, NEGR1, SEC16B, TMEM18 |
| Reactome | Unfolded Protein Response | 2, 3e, 4e, 40e | DCP2, SSR1, WFS1, PLA2G4B, ASNS |
| KEGG | Insulin signaling pathway | 3e, 4e | FLOT1, PPP1R3B, FBP2, GCK, HK1, IRS1, MAP2K1, MAPK3 |
| Reactome | Activation of Chaperones by IRE1alpha | 2, 4e, 40e | DDX11, SSR1, WFS1 |
| KEGG | Maturity onset diabetes of the young | 1, 2, 3e | GCK, HHEX, SLC2A2, BHLHA15, HNF1A, HNF1B, HNF4A, MNX1, NEUROG3 |
| KEGG | Acute myeloid leukemia | 1, 2 | MAPK3, STAT3, TCF7L2, CHUK, FLT3, RELA |
| Reactome | Nuclear Receptor transcription pathway | 3e, 4e | NR1H3, NR5A2, PPARG |
| KEGG | Type II diabetes mellitus | 3e | ABCC8, GCK, HK1, IRS1, KCNJ11, MAPK3 |
| BioCarta | Insulin Signaling Pathway | 3e, 4e | IRS1, MAP2K1, MAPK3, RAF1 |
| Reactome | Incretin Synthesis, Secretion, and Inactivation | 1, 2 | GIP, TCF7L2, GATA4, CDX2 |
| Reactome | Synthesis, Secretion, and Inactivation of Glucagon-like Peptide-1 (GLP-1) | 1, 2 | TCF7L2, CDX2 |
| Reactome | Regulation of beta-cell development | 1, 2 | GCK, HNF1A, HNF1B, HNF4A, NEUROG3, NR5A2, PDX1, SLC2A2 |
| BioCarta | Integrin Signaling Pathway | 1 | ACTA1, ACTN1, BCAR1, ITGA1, MAPK3, MAPK8 |
| BioCarta | TNF/Stress Related Signaling | 1 | CHUK, LTA, MAP3K1, MAPK8, RELA, TNF |
| Reactome | Transport of glucose and other sugars, bile salts and organic acids, metal ions and amine compounds | 4e | SLC44A4, SLC22A18, SLC2A2, SLC22A7 |
| Reactome | ABC-family proteins mediated transport | 5e | ABCC5, CFTR, ABCB10 |
| Reactome | Regulation of gene expression in beta cells | 1 | GCK, HNF1A, HNF4A, PDX1, SLC2A2 |
| KEGG | Basal cell carcinoma | 1 | DVL3, TCF7L2 |
| Reactome | Zinc transporters | 1 | SLC30A8 |
| BioCarta | Cystic Fibrosis Transmembrane Conductance Regulator And Beta 2 Adrenergic Receptor Pathway | 1 | PRKAR1A |
| Reactome | Synthesis, Secretion, and Inactivation of Glucose-dependent Insulinotropic Polypeptide (GIP) | 1 | GIP, ISL1, GATA4, DPP4 |
| Reactome | Aquaporin-mediated transport | 1 | ADCY5, GNG13, AQP7 |

## Figures

### Figure 1. Shared genetic mechanisms between AD and T2D: Study overview

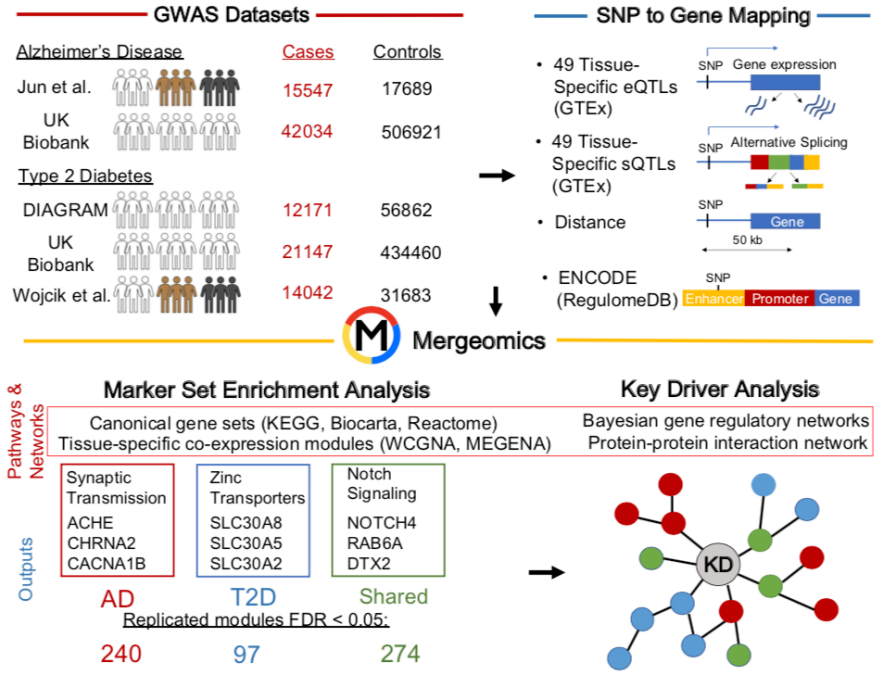


**Figure 2. Summary of significant pathways/modules replicated across GWAS studies and informative tissue-specific mapping methods.**
Numbers within bars represent numbers of replicated modules across at least two studies. Text below 'Shared' bars refer to select shared modules between AD and T2D.

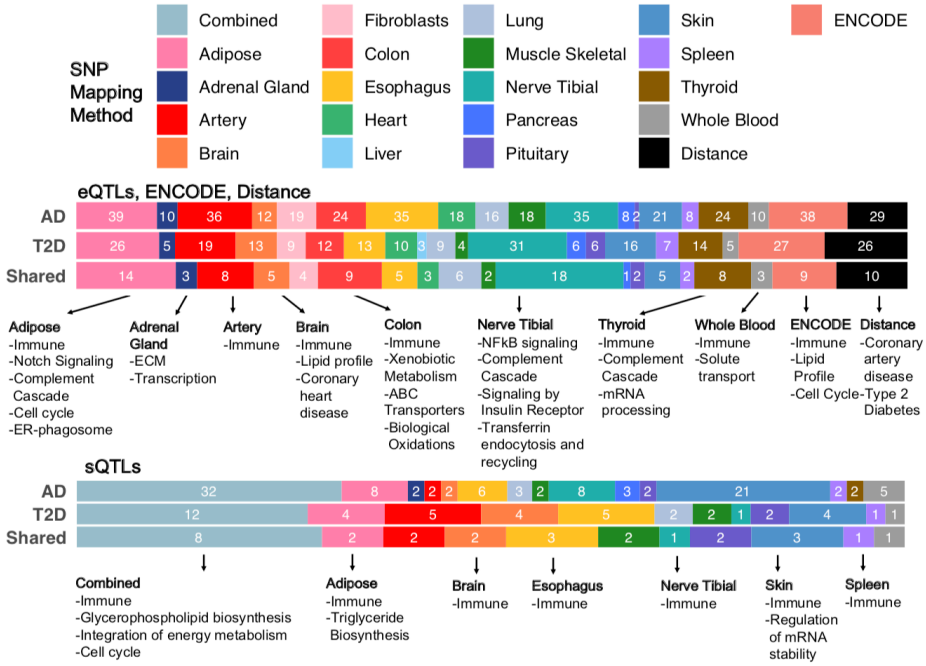

**Figure 3. Shared subnetworks between AD and T2D revealed by peripheral and brain eQTL mapping methods overlaid with a combined Bayesian multi-tissue gene regulatory network.**

Key drivers are shown as the biggest nodes. Edge color denotes tissues specificity. Node color denotes genes that were mapped from SNPs and members of significantly associated modules. Node border denotes whether a gene was a GWAS hit for either AD or T2D or both.

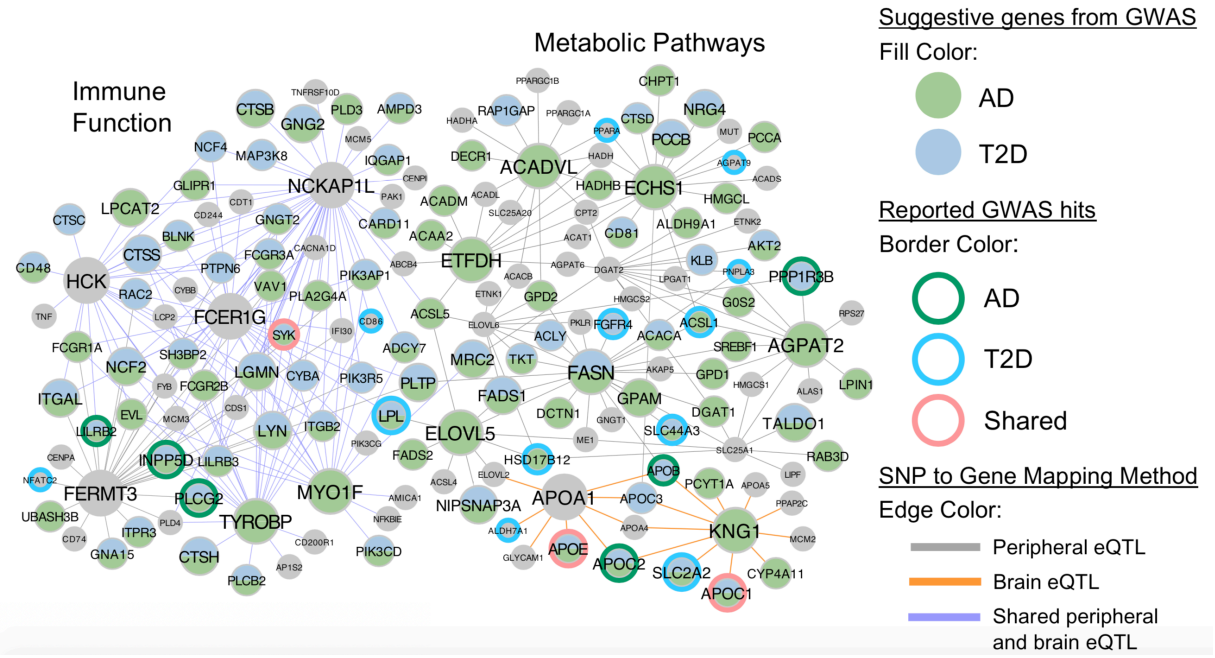

**Figure 4. Cell type identification and global transcriptional shifts of 5XFAD cells.** tSNE plots are colored by cell type and by condition. Cell type proportion plots show relative distributions of cell type numbers by sample. Euclidean distance plot shows magnitude of overall transcriptional change between WT and 5XFAD cells for each cell type. Cell marker plot shows gene expression of 8 markers per major cell type in both tissues and in both conditions.

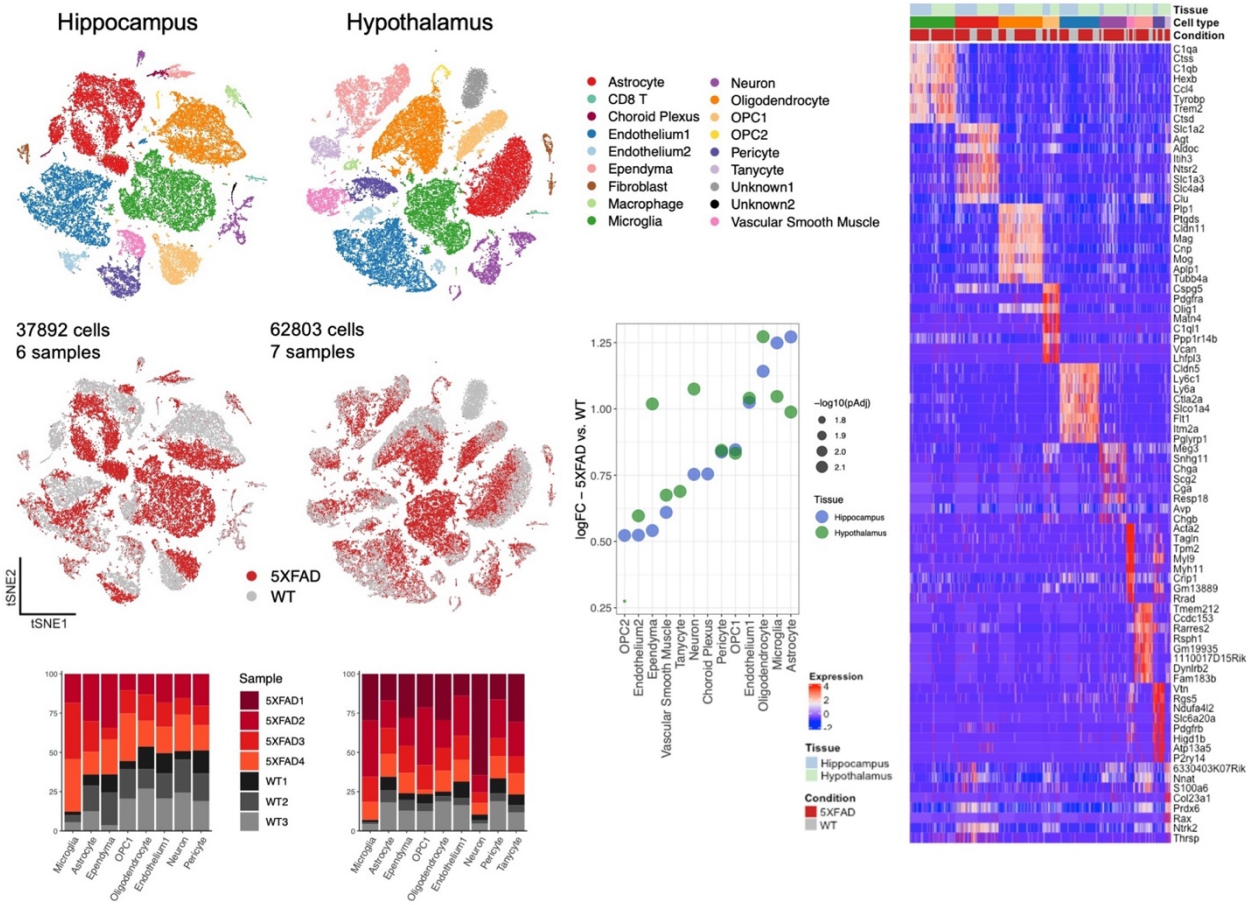

**Figure 5. Top gene and pathway disruptions induced by amyloidosis (5XFAD status).** LogFC is log fold change. Positive logFC is red (point fill color) and means higher expression in 5XFAD. Negative logFC is blue and means lower expression in 5XFAD. Higher intensity of the color means larger change. $P_{adj}$ is adjusted p value. Size of the point refers to the magnitude of significance. The larger the point, the higher the significance. The shape of the point designates whether the change is significant. The point is a diamond if the change is FDR>0.05 and a circle if the change is FDR<0.05 (significant). The absence of a point means no change. In the bottom plot, the summed logFCs of individual pathway gene members is shown in the heatmap.

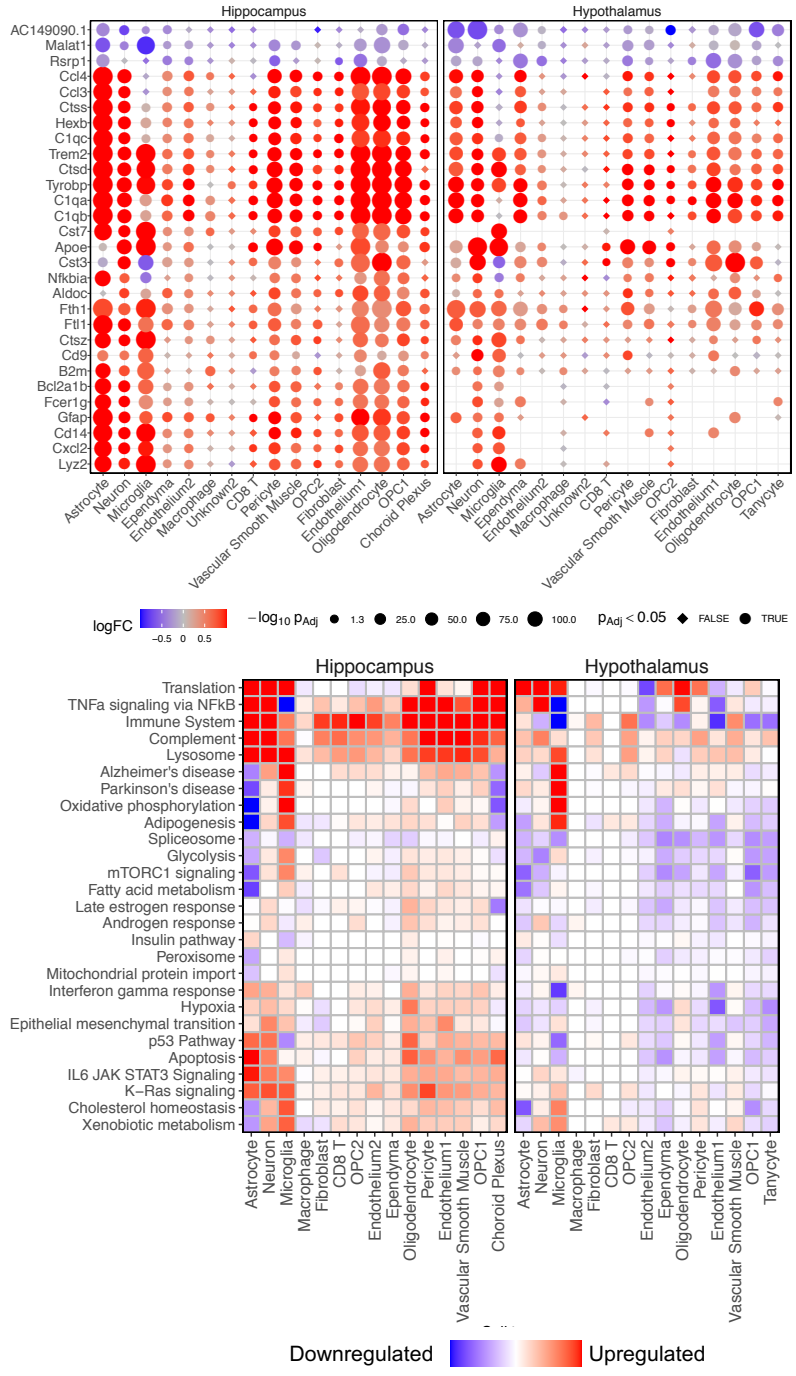

**Figure 6. Cell-type specific differentially expressed genes (DEGs).**
On the left are cell type specific DEGs shared between hippocampus and hypothalamus. On the right are cell-type and tissue specific DEGs. LogFC is log fold change. Positive logFC is red (point fill color) and means higher expression in 5XFAD. Negative logFC is blue and means lower expression in 5XFAD. Higher intensity of the color means larger change. $P_{adj}$ is adjusted p value. Size of the point refers to the magnitude of significance. The larger the point, the higher the significance. The shape of the point designates whether the change is significant. The point is a diamond if the change is FDR>0.05 and a circle if the change is FDR<0.05 (significant). The absence of a point means no change.

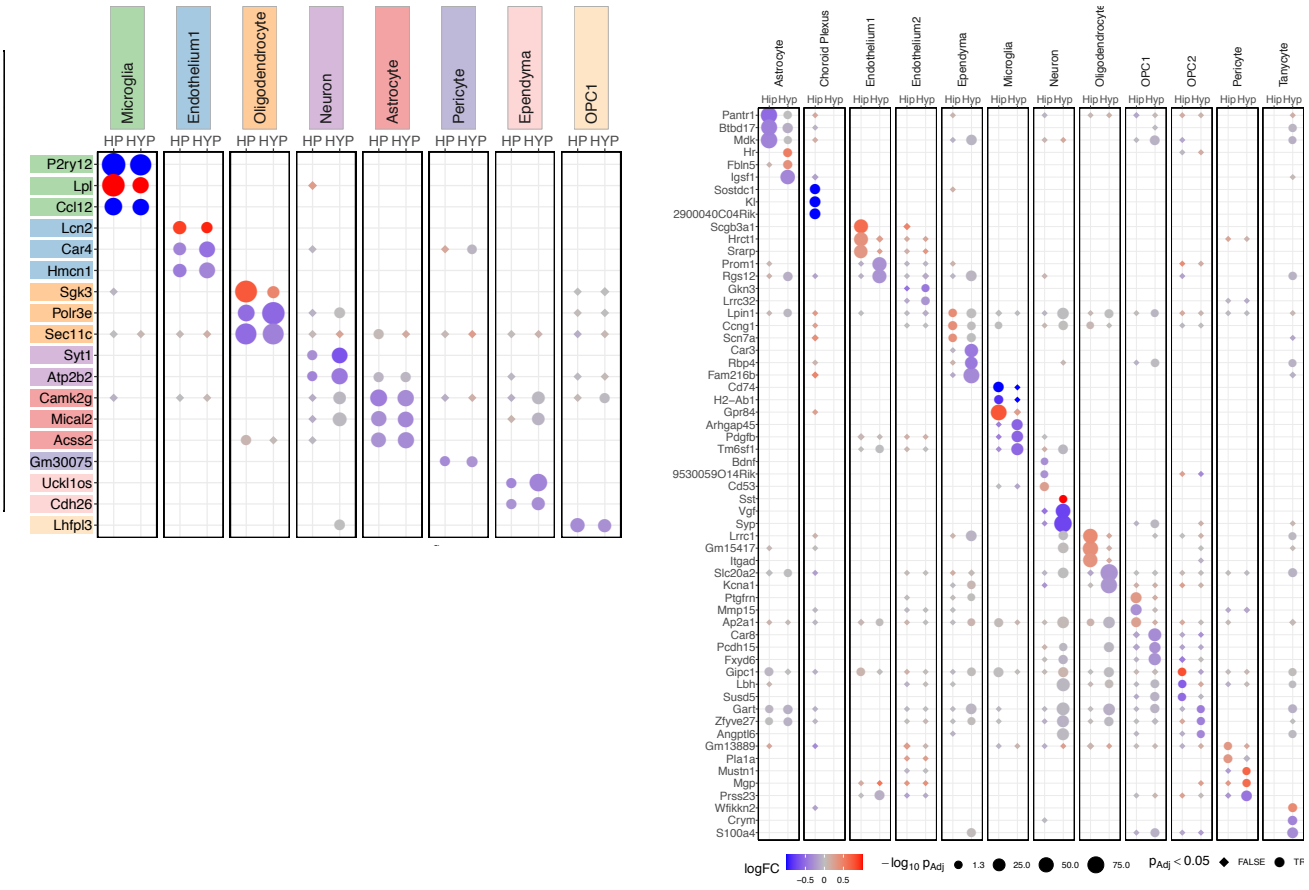

**Figure 7. Tissue specific DEGs.**
LogFC is log fold change. Positive logFC is red (point fill color) and means higher expression in 5XFAD. Negative logFC is blue and means lower expression in 5XFAD. Higher intensity of the color means larger change. $P_{adj}$ is adjusted p value. Size of the point refers to the magnitude of significance. The larger the point, the higher the significance. The shape of the point designates whether the change is significant. The point is a diamond if the change is FDR>0.05 and a circle if the change is FDR<0.05 (significant). The absence of a point means no change.

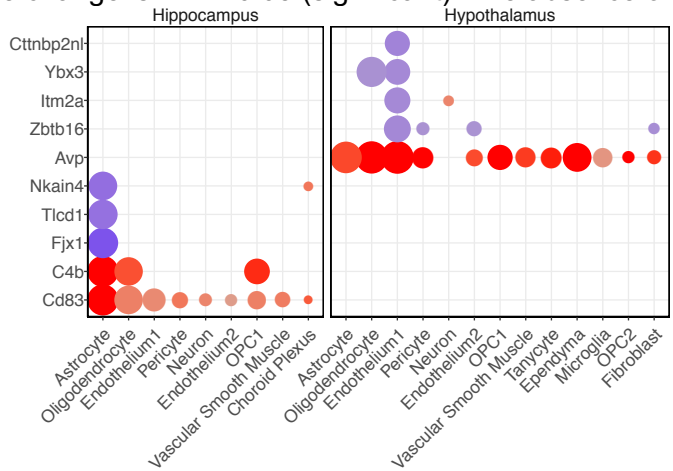


**Figure 8. Differential gene responses across cell types to the 5XFAD condition.**
Positive logFC is red (point fill color) and means higher expression in 5XFAD. Negative logFC is blue and means lower expression in 5XFAD. Higher intensity of the color means larger change. $P_{adj}$ is adjusted p value. Size of the point refers to the magnitude of significance. The larger the point, the higher the significance. The shape of the point designates whether the change is significant. The point is a diamond if the change is FDR>0.05 and a circle if the change is FDR<0.05 (significant). The absence of a point means no change.

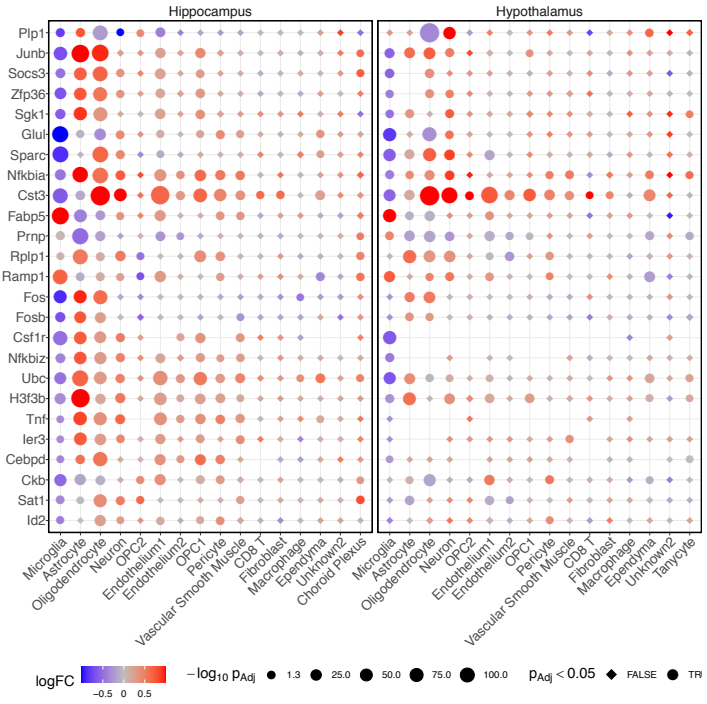

**Figure 9. Secreted-peptide cell-cell communication in WT and 5XFAD cells.**
Intensity of fill signifies the significance of the interaction. The numbers in the heatmap show the score of the interaction (higher gene-gene co-expressions between source and target cell types give higher scores). On the bottom axis are the source cell types and on the left axis are the target cell types.

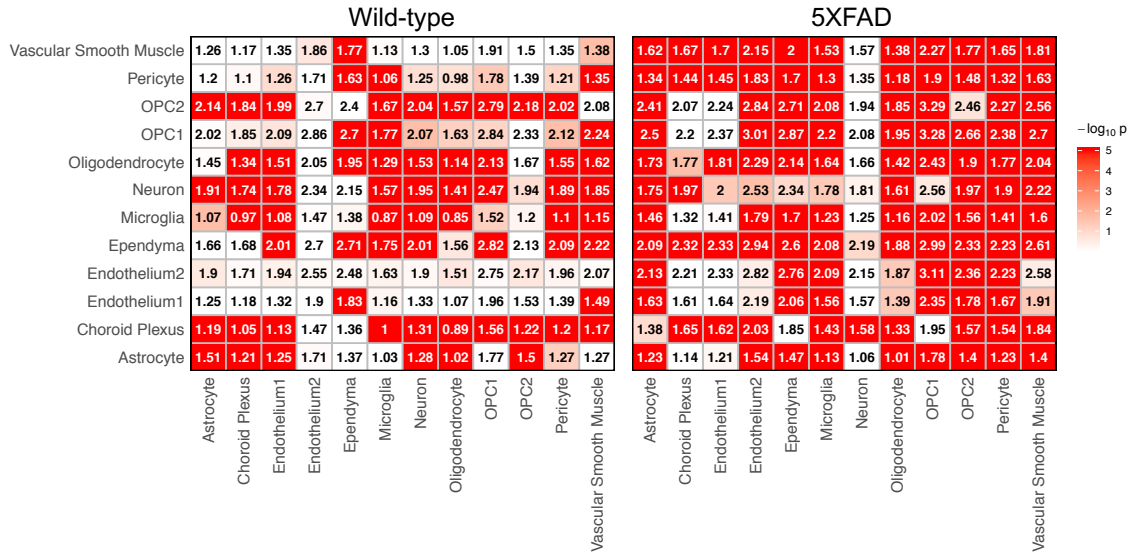


**Figure 10. GWAS Enrichment of cell-type specific 5XFAD differentially expressed genes from the hippocampus.**
Number of DEGs for each cell type is shown next to the cell type name on the left side. Number of cases for GWAS studies shown next to study name at the bottom. The fill intensity shows the strength of significance and asterisks indicate enrichments that have an FDR<0.05.

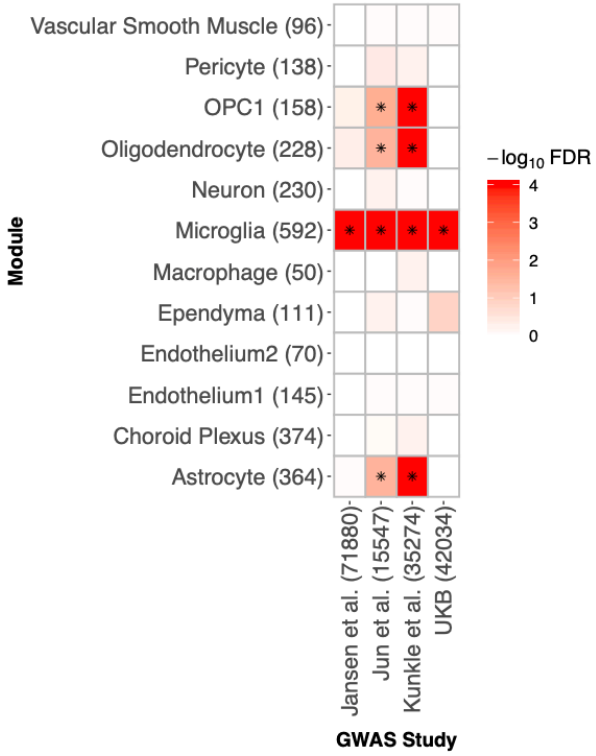

**Figure 11. Pseudotime analysis of 5XFAD microglial activation using Slingshot.** Computed clusters are shown on the top left and predicted trajectory along these cluster is shown on the bottom right. Darker colors on the trajectory gradient represent the “beginning” of the trajectory. Expression of 500 genes significantly changing as a function of pseudotime and grouped into 15 categories are plotted in the middle heatmap. Pathway enrichment of these 15 categories is shown on the right heatmap. The fill intensity is the enrichment value. The numbers in the heatmap show the number of overlapped genes with the pathway. The black border denotes a significant enrichment (FDR<0.05). The numbers adjacent to the pseudotime group name are the number of genes in that category.

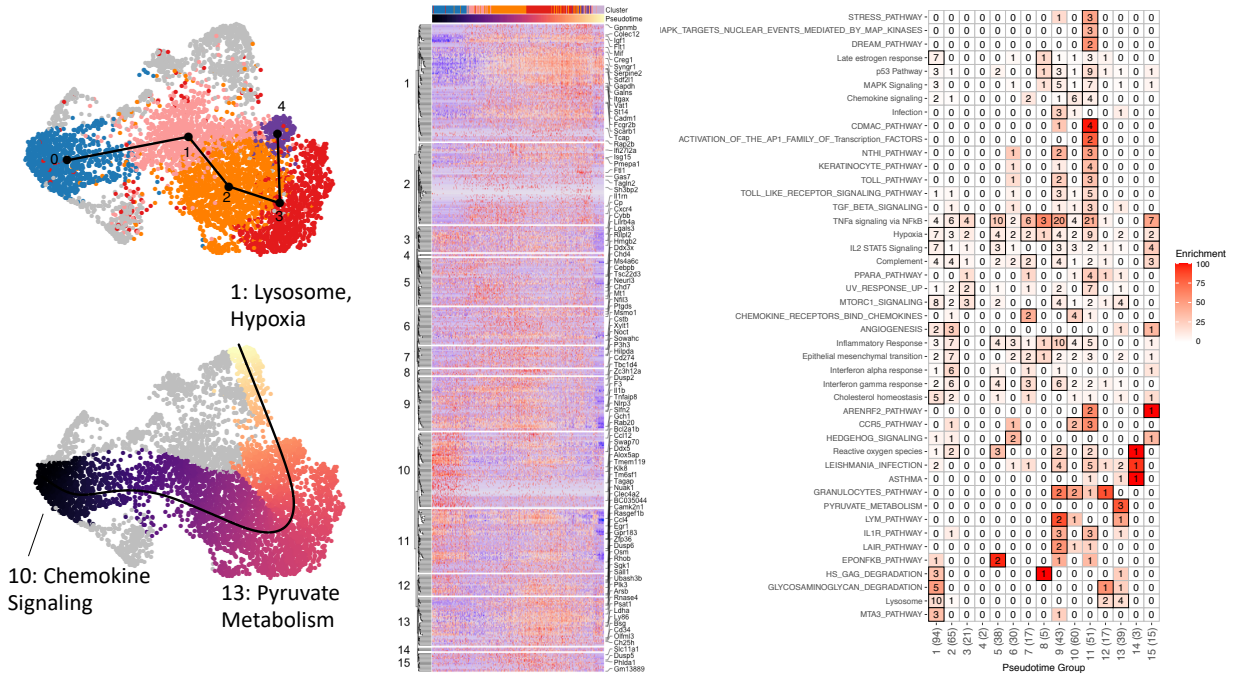

**Figure 12. Neuronal sub-clustering for hippocampus and hypothalamus.**
Clustering of neurons is shown on the left. Marker gene expression of hippocampal neurons is shown in the top middle. Hippocampal sub-cluster top DEGs are shown on the top right. All gene expression changes between 5XFAD and WT in hypothalamic neurons is shown on the bottom right. For the dot plots, positive logFC is red (point fill color) and means higher expression in 5XFAD. Negative logFC is blue and means lower expression in 5XFAD. Higher intensity of the color means larger change. $P_{adj}$ is adjusted p value. Size of the point refers to the magnitude of significance. The larger the point, the higher the significance. The shape of the point designates whether the change is significant. The point is a diamond if the change is FDR>0.05 and a circle if the change is FDR<0.05 (significant). The absence of a point means no change.

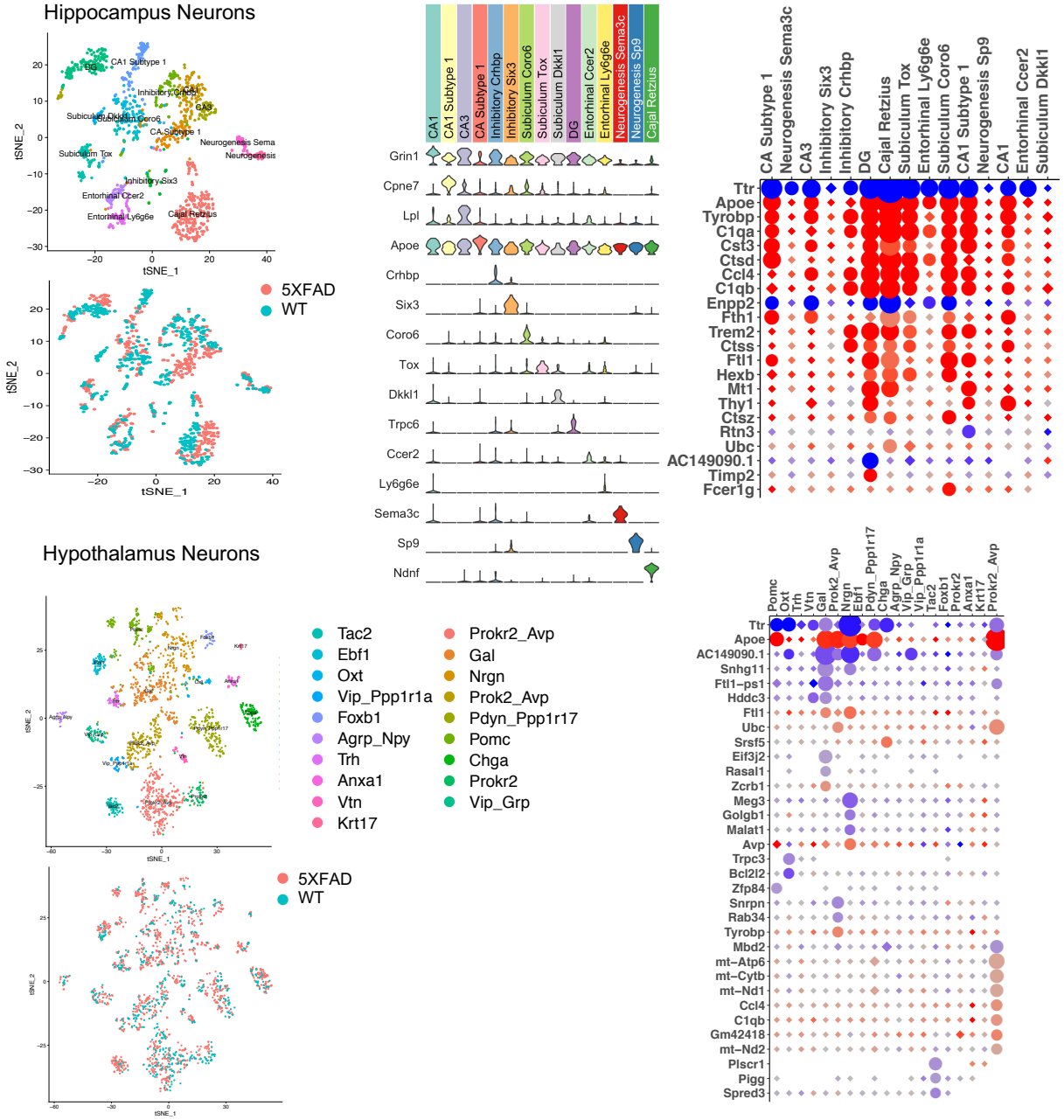

**Figure 13. Effect of fructose on top AD pathways in the hippocampus.**
The intensity of the fill reflects number of genes overlapped in the pathway that were either downregulated or upregulated. “AD” is the comparison 5XFAD versus WT. “F” is the comparison 5XFAD with fructose versus 5XFAD.

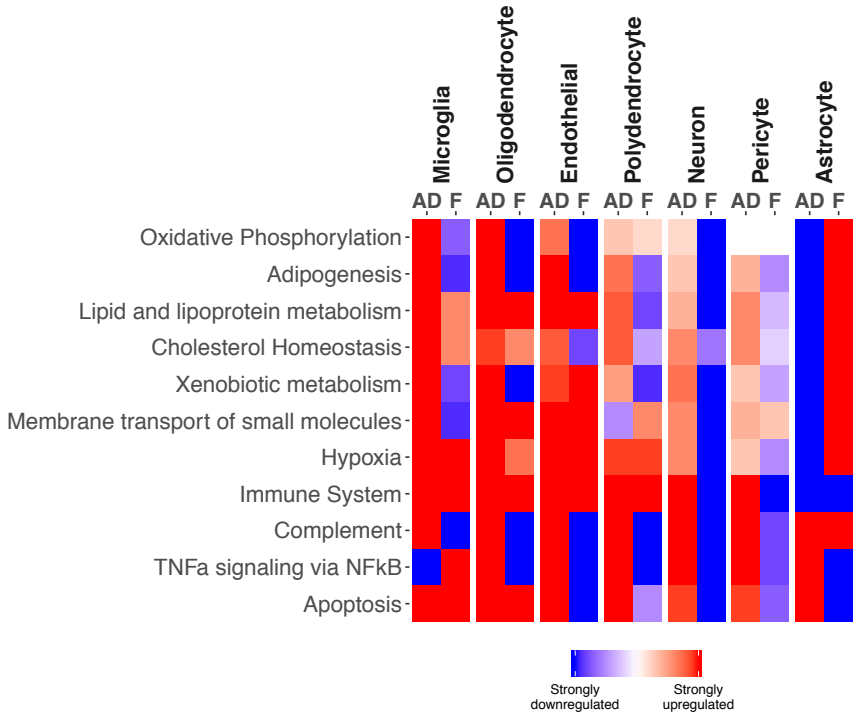


**Figure 14. Differential effects of 5XFAD transgenic status and fructose in neurons of the hippocampus and hypothalamus.**
The intensity of the fill reflects number of genes overlapped in the pathway that were either downregulated or upregulated. “AD” is the comparison 5XFAD versus WT. “F” is the comparison 5XFAD with fructose versus 5XFAD. “HP” is hippocampus. “HYP” is hypothalamus.

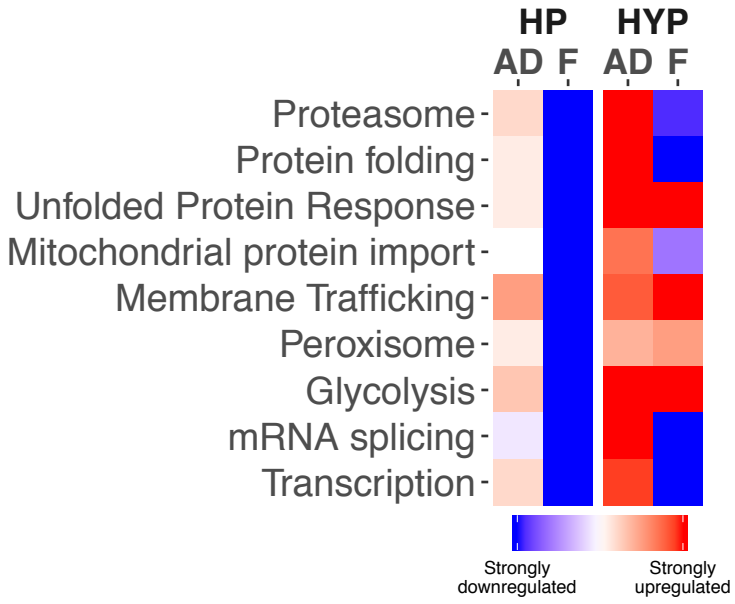

**Figure 15. Effect of dietary interventions on a subset of GWAS genes.** Positive logFC is red (point fill color) and means higher expression in 5XFAD. Negative logFC is blue and means lower expression in 5XFAD. Higher intensity of the color means larger change. $P_{adj}$ is adjusted p value. Size of the point refers to the magnitude of significance. The larger the point, the higher the significance. The shape of the point designates whether the change is significant. The point is a diamond if the change is FDR>0.05 and a circle if the change is FDR<0.05 (significant). The absence of a point means no change. “Fructose on AD” is the comparison 5XFAD with fructose versus 5XFAD. “DHA on AD+Fructose” is the comparison 5XFAD with fructose and DHA versus 5XFAD with fructose. “NR on AD+Fructose” is the comparison 5XFAD with fructose and NR versus 5XFAD with fructose.

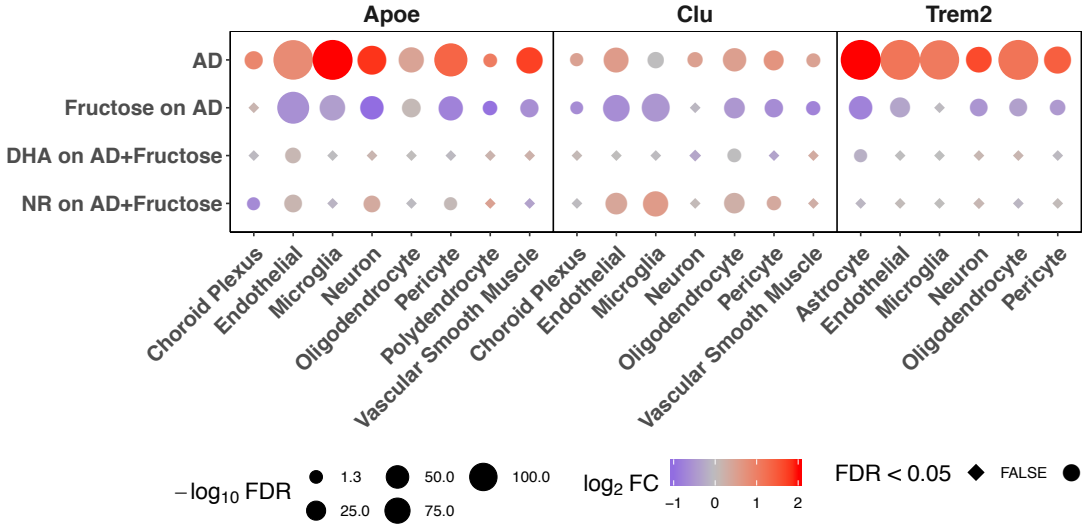


**Figure 16. Effect of dietary interventions on top differentially expressed genes in 5XFAD.** Positive logFC is red (point fill color) and means higher expression in 5XFAD. Negative logFC is blue and means lower expression in 5XFAD. Higher intensity of the color means larger change. $P_{adj}$ is adjusted p value. Size of the point refers to the magnitude of significance. The larger the point, the higher the significance. The shape of the point designates whether the change is significant. The point is a diamond if the change is FDR>0.05 and a circle if the change is FDR<0.05 (significant). The absence of a point means no change. “DHA on AD+Fructose” is the comparison 5XFAD with fructose and DHA versus 5XFAD with fructose. “NR on AD+Fructose” is the comparison 5XFAD with fructose and NR versus 5XFAD with fructose. “DHA+Fructose on AD” is the comparison 5XFAD with fructose and DHA versus 5XFAD. “NR+Fructose on AD” is the comparison 5XFAD with fructose and NR versus 5XFAD.

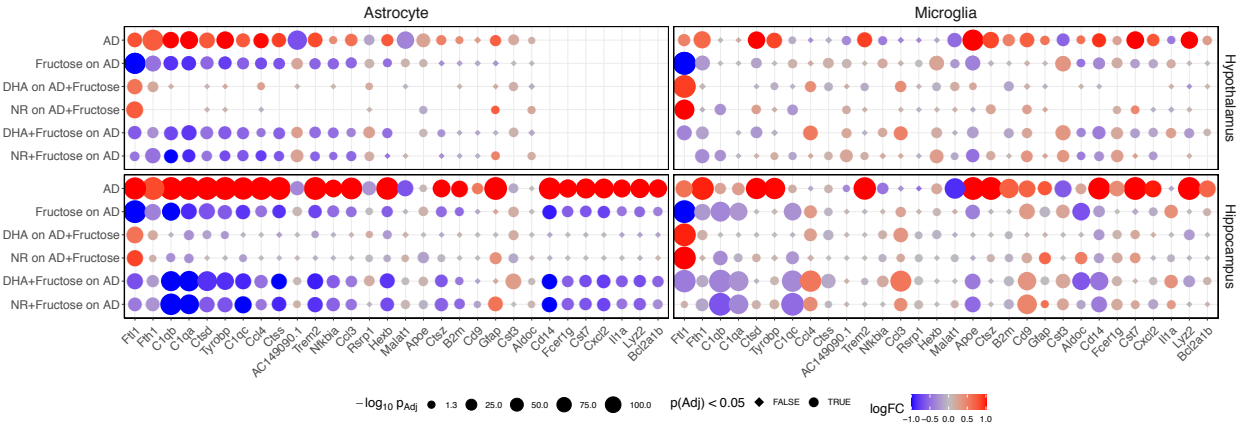

**Figure 17. Pathway alterations caused by nutritional interventions.** The comparisons denoted on the top are as follows: 5XFAD versus wild-type (AD), 5XFAD with fructose versus 5XFAD (Fructose on AD), 5XFAD with fructose and NR versus 5XFAD (NR and Fructose on AD), 5XFAD with fructose and DHA versus 5XFAD (DHA and Fructose on AD). These pathways emphasize those that were minimally affected by fructose alone but were significantly affected in NR and fructose or DHA and fructose. This serves as a quasi "effect of NR"/"effect of DHA" alone when comparing the pathway response between "Fructose on AD" and "DHA and Fructose on AD"/"NR and Fructose on AD". The size of the dot represents the enrichment of the pathway with DEGs. Larger dot size means higher enrichment of the pathway. A black border around the dot means the enrichment is significant (FDR is less than 0.05). The intensity of the color represents the number of genes that were up- or downregulated. For all pathways shown, there was a clear upregulation or clear downregulation (most or all genes were downregulated or upregulated).

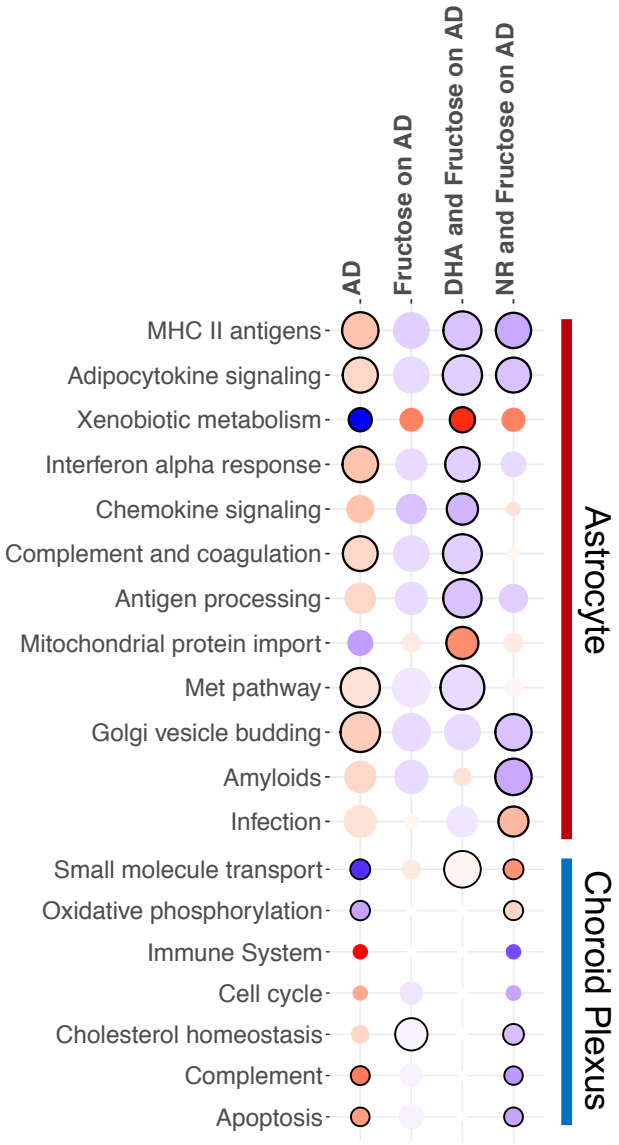

**Figure 18. Connectivity map drug repositioning informed by cell-type specific differentially expressed genes in 5XFAD.** Shown are the top predicted drugs with each drug having a 'Connectivity Score' in at least one cell type that is over 95 (max score is 100).

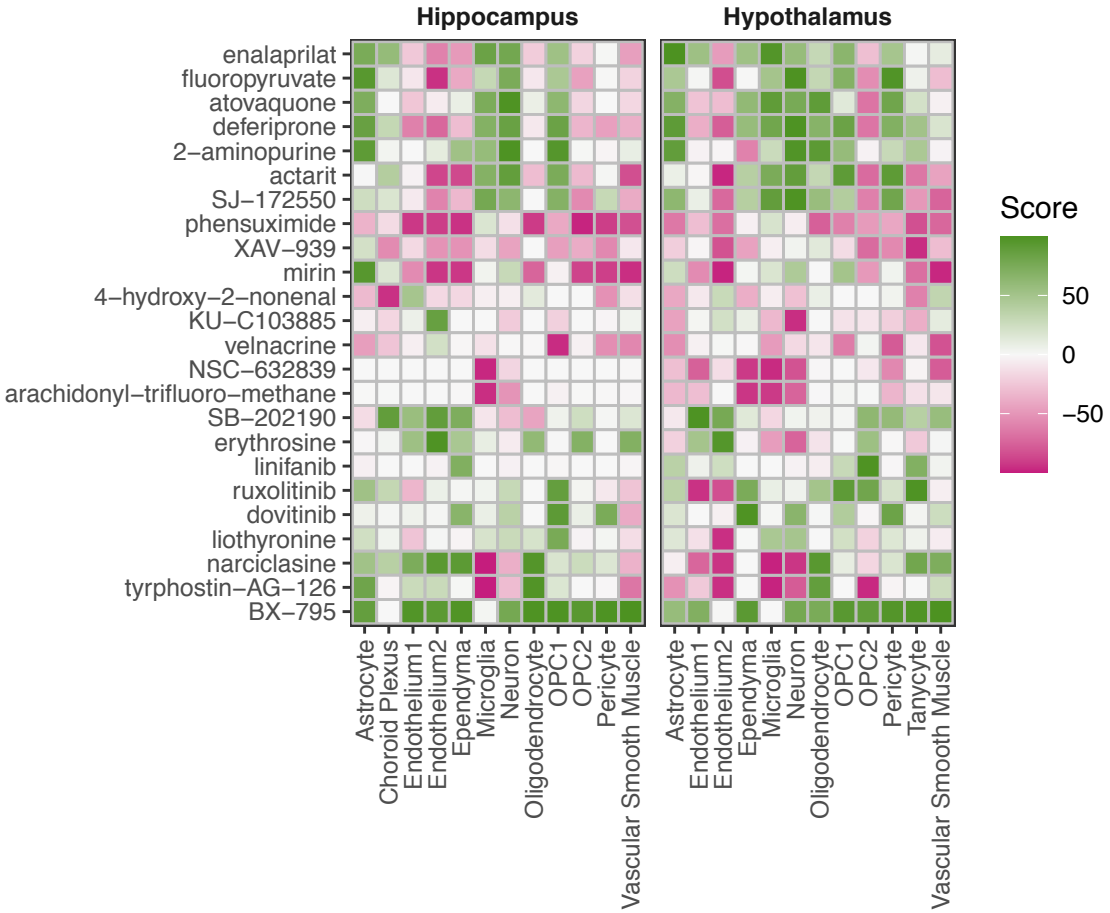

## References


1 Butterfield, D. A. & Halliwell, B. Oxidative stress, dysfunctional glucose metabolism and Alzheimer disease. *Nature Reviews Neuroscience* **20**, 148-160, doi:10.1038/s41583-019-0132-6 (2019).

2 Heneka, M. T. *et al.* Neuroinflammation in Alzheimer's disease. *The Lancet Neurology* **14**, 388-405, doi:10.1016/S1474-4422(15)70016-5 (2015).

3 Mosconi, L. Glucose metabolism in normal aging and Alzheimer's disease: Methodological and physiological considerations for PET studies. *Clin Transl Imaging* **1**, 10.1007/s40336-40013-40026-y, doi:10.1007/s40336-013-0026-y (2013).

4 Swerdlow, R. H. Mitochondria and Mitochondrial Cascades in Alzheimer's Disease. *J Alzheimers Dis* **62**, 1403-1416, doi:10.3233/JAD-170585 (2018).

5 Zatta, P., Drago, D., Bolognin, S. & Sensi, S. L. Alzheimer's disease, metal ions and metal homeostatic therapy. *Trends in Pharmacological Sciences* **30**, 346-355, doi:https://doi.org/10.1016/j.tips.2009.05.002 (2009).

6 Arnold, S. E. *et al.* Brain insulin resistance in type 2 diabetes and Alzheimer disease: concepts and conundrums. *Nat Rev Neurol* **14**, 168-181, doi:10.1038/nrneurol.2017.185 (2018).

7 Raji, C. A. *et al.* Brain structure and obesity. *Hum Brain Mapp* **31**, 353-364, doi:10.1002/hbm.20870 (2010).

8 Newcomer, J. W. Metabolic syndrome and mental illness. *Am J Manag Care* **13**, S170-177 (2007).

9 Farooqui, A. A., Farooqui, T., Panza, F. & Frisardi, V. Metabolic syndrome as a risk factor for neurological disorders. *Cell Mol Life Sci* **69**, 741-762, doi:10.1007/s00018-011-0840-1 (2012).

10 Haffner, S. & Taegtmeyer, H. Epidemic obesity and the metabolic syndrome. *Circulation* **108**, 1541-1545, doi:10.1161/01.Cir.0000088845.17586.Ec (2003).

11 Schmoller, A. *et al.* Evidence for a Relationship between Body Mass and Energy Metabolism in the Human Brain. *Journal of Cerebral Blood Flow & Metabolism* **30**, 1403-1410, doi:10.1038/jcbfm.2010.48 (2010).

12 Zhang, L. *et al.* Diet-induced metabolic disturbances as modulators of brain homeostasis. *Biochim Biophys Acta* **1792**, 417-422, doi:10.1016/j.bbadis.2008.09.006 (2009).

13 Kroner, Z. The relationship between Alzheimer's disease and diabetes: Type 3 diabetes? *Altern Med Rev* **14**, 373-379 (2009).

14 Clarke, J. R., Ribeiro, F. C., Frozza, R. L., De Felice, F. G. & Lourenco, M. V. Metabolic Dysfunction in Alzheimer's Disease: From Basic Neurobiology to Clinical Approaches. *Journal of Alzheimer's Disease* **64**, S405-S426, doi:10.3233/JAD-179911 (2018).

15 Demarest, T. G. *et al.* Biological sex and DNA repair deficiency drive Alzheimer's disease via systemic metabolic remodeling and brain mitochondrial dysfunction. *Acta Neuropathol*, doi:10.1007/s00401-020-02152-8 (2020).

16 Kang, S., Lee, Y. H. & Lee, J. E. Metabolism-Centric Overview of the Pathogenesis of Alzheimer's Disease. *Yonsei Med J* **58**, 479-488, doi:10.3349/ymj.2017.58.3.479 (2017).

17 Yang, X. Multitissue Multiomics Systems Biology to Dissect Complex Diseases. *Trends in Molecular Medicine*, doi:https://doi.org/10.1016/j.molmed.2020.04.006 (2020).

18 Stančáková, A. & Laakso, M. Genetics of Type 2 Diabetes. *Endocrine Development* **31**, 203-220, doi:10.1159/000439418 (2016).

19 Sun, Q., Xie, N., Tang, B., Li, R. & Shen, Y. Alzheimer's Disease: From Genetic Variants to the Distinct Pathological Mechanisms. *Frontiers in Molecular Neuroscience* **10**, 319 (2017).

20 Van Cauwenberghe, C., Van Broeckhoven, C. & Sleegers, K. The genetic landscape of Alzheimer disease: clinical implications and perspectives. *Genetics in Medicine* **18**, 421-430, doi:10.1038/gim.2015.117 (2016).

21 Wang, X. *et al.* Genetic markers of type 2 diabetes: Progress in genome-wide association studies and clinical application for risk prediction. *Journal of Diabetes* **8**, 24-35, doi:10.1111/1753-0407.12323 (2016).

22 González-Domínguez, R., García-Barrera, T., Vitorica, J. & Gómez-Ariza, J. L. Region-specific metabolic alterations in the brain of the APP/PS1 transgenic mice of Alzheimer's disease. *Biochimica et Biophysica Acta (BBA) - Molecular Basis of Disease* **1842**, 2395-2402, doi:https://doi.org/10.1016/j.bbadis.2014.09.014 (2014).

23 Wakabayashi, T. *et al.* Differential effects of diet- and genetically-induced brain insulin resistance on amyloid pathology in a mouse model of Alzheimer's disease. *Molecular Neurodegeneration* **14**, 15, doi:10.1186/s13024-019-0315-7 (2019).

24 2020 Alzheimer's disease facts and figures. *Alzheimer's & Dementia* **16**, 391-460, doi:10.1002/alz.12068 (2020).

25 IDF Diabetes Atlas 9th Edition. (International Diabetes Federation, 2019).

26 Mittal, K. & Katare, D. P. Shared links between type 2 diabetes mellitus and Alzheimer's disease: A review. *Diabetes Metab Syndr* **10**, S144-149, doi:10.1016/j.dsx.2016.01.021 (2016).

27 Freude, S. *et al.* Peripheral hyperinsulinemia promotes tau phosphorylation in vivo. *Diabetes* **54**, 3343-3348, doi:10.2337/diabetes.54.12.3343 (2005).

28 Mullins, R. J., Diehl, T. C., Chia, C. W. & Kapogiannis, D. Insulin Resistance as a Link between Amyloid-Beta and Tau Pathologies in Alzheimer's Disease. *Front Aging Neurosci* **9**, 118-118, doi:10.3389/fnagi.2017.00118 (2017).

29 McNay, E. C. *et al.* Hippocampal memory processes are modulated by insulin and high-fat-induced insulin resistance. *Neurobiol Learn Mem* **93**, 546-553, doi:10.1016/j.nlm.2010.02.002 (2010).

30 Hao, K. *et al.* Shared genetic etiology underlying Alzheimer's disease and type 2 diabetes. *Mol Aspects Med* **43-44**, 66-76, doi:10.1016/j.mam.2015.06.006 (2015).

31 Wang, X. F. *et al.* Linking Alzheimer's disease and type 2 diabetes: Novel shared susceptibility genes detected by cFDR approach. *J Neurol Sci* **380**, 262-272, doi:10.1016/j.jns.2017.07.044 (2017).

32 Zhu, Z., Lin, Y., Li, X., Driver, J. A. & Liang, L. Shared genetic architecture between metabolic traits and Alzheimer's disease: a large-scale genome-wide cross-trait analysis. *Hum Genet* **138**, 271-285, doi:10.1007/s00439-019-01988-9 (2019).

33 Shu, L. *et al.* Shared genetic regulatory networks for cardiovascular disease and type 2 diabetes in multiple populations of diverse ethnicities in the United States. *PLoS Genet* **13**, e1007040, doi:10.1371/journal.pgen.1007040 (2017).

34 Shu, L. *et al.* Mergeomics: multidimensional data integration to identify pathogenic perturbations to biological systems. *BMC Genomics* **17**, 874, doi:10.1186/s12864-016-3198-9 (2016).

35 Boyle, E. A., Li, Y. I. & Pritchard, J. K. An Expanded View of Complex Traits: From Polygenic to Omnigenic. *Cell* **169**, 1177-1186, doi:10.1016/j.cell.2017.05.038 (2017).

36 Arneson, D., Bhattacharya, A., Shu, L., Mäkinen, V.-P. & Yang, X. Mergeomics: a web server for identifying pathological pathways, networks, and key regulators via multidimensional data integration. *BMC Genomics* **17**, 722, doi:10.1186/s12864-016-3057-8 (2016).

37 Scott, R. A. *et al.* An Expanded Genome-Wide Association Study of Type 2 Diabetes in Europeans. *Diabetes* **66**, 2888-2902, doi:10.2337/db16-1253 (2017).

38 Xue, A. *et al.* Genome-wide association analyses identify 143 risk variants and putative regulatory mechanisms for type 2 diabetes. *Nat Commun* **9**, 2941, doi:10.1038/s41467-018-04951-w (2018).

39 Wojcik, G. L. *et al.* Genetic analyses of diverse populations improves discovery for complex traits. *Nature* **570**, 514-518, doi:10.1038/s41586-019-1310-4 (2019).

40 Jun, G. R. *et al.* Transethnic genome-wide scan identifies novel Alzheimer's disease loci. *Alzheimer's & Dementia* **13**, 727-738, doi:https://doi.org/10.1016/j.jalz.2016.12.012 (2017).

41 Marioni, R. E. *et al.* GWAS on family history of Alzheimer's disease. *Translational Psychiatry* **8**, 99, doi:10.1038/s41398-018-0150-6 (2018).

42 Aguet, F. *et al.* Genetic effects on gene expression across human tissues. *Nature* **550**, 204-213, doi:10.1038/nature24277 (2017).

43 The ENCODE (ENCyclopedia Of DNA Elements) Project. *Science* **306**, 636-640, doi:10.1126/science.1105136 (2004).

44 Kanehisa, M. & Goto, S. KEGG: kyoto encyclopedia of genes and genomes. *Nucleic Acids Res* **28**, 27-30, doi:10.1093/nar/28.1.27 (2000).

45 Fabregat, A. *et al.* Reactome pathway analysis: a high-performance in-memory approach.

46 Nishimura, D. BioCarta. *Biotech Software & Internet Report* **2**, 117-120, doi:10.1089/152791601750294344 (2001).

47 Langfelder, P. & Horvath, S. WGCNA: an R package for weighted correlation network analysis. *BMC Bioinformatics* **9**, 559, doi:10.1186/1471-2105-9-559 (2008).

48 Song, W.-M. & Zhang, B. Multiscale Embedded Gene Co-expression Network Analysis. *PLOS Computational Biology* **11**, e1004574, doi:10.1371/journal.pcbi.1004574 (2015).

49 Zhu, J. *et al.* Increasing the Power to Detect Causal Associations by Combining Genotypic and Expression Data in Segregating Populations. *PLOS Computational Biology* **3**, e69, doi:10.1371/journal.pcbi.0030069 (2007).

50 Shannon, P. *et al.* Cytoscape: a software environment for integrated models of biomolecular interaction networks. *Genome Res* **13**, 2498-2504, doi:10.1101/gr.1239303 (2003).

51 Chen, Y.-W. *et al.* PharmOmics: A Species- and Tissue-specific Drug Signature Database and Online Tool for Toxicity Prediction and Drug Repurposing. *bioRxiv*, 837773, doi:10.1101/837773 (2019).

52 Cao, W. & Zheng, H. Peripheral immune system in aging and Alzheimer's disease. *Molecular Neurodegeneration* **13**, 51, doi:10.1186/s13024-018-0284-2 (2018).

53 Kinney, J. W. *et al.* Inflammation as a central mechanism in Alzheimer's disease. *Alzheimer's & Dementia: Translational Research & Clinical Interventions* **4**, 575-590, doi:https://doi.org/10.1016/j.trci.2018.06.014 (2018).

54 Stephens, H. A. F. MICA and MICB genes: can the enigma of their polymorphism be resolved? *Trends in Immunology* **22**, 378-385, doi:10.1016/S1471-4906(01)01960-3 (2001).

55 Garranzo-Asensio, M. *et al.* Identification of prefrontal cortex protein alterations in Alzheimer's disease. *Oncotarget* **9** (2018).

56 Dominy, S. S. *et al.* <em>Porphyromonas gingivalis</em> in Alzheimer's disease brains: Evidence for disease causation and treatment with small-molecule inhibitors. *Science Advances* **5**, eaau3333, doi:10.1126/sciadv.aau3333 (2019).

57 Gastaldi, G., Goossens, N., Clément, S. & Negro, F. Current level of evidence on causal association between hepatitis C virus and type 2 diabetes: A review. *Journal of Advanced Research* **8**, 149-159, doi:https://doi.org/10.1016/j.jare.2016.11.003 (2017).

58 Sochocka, M., Zwolińska, K. & Leszek, J. The Infectious Etiology of Alzheimer's Disease. *Curr Neuropharmacol* **15**, 996-1009, doi:10.2174/1570159X15666170313122937 (2017).

59 Warner, M. S. *et al.* A Cell Surface Protein with Herpesvirus Entry Activity (HveB) Confers Susceptibility to Infection by Mutants of Herpes Simplex Virus Type 1, Herpes Simplex Virus Type 2, and Pseudorabies Virus. *Virology* **246**, 179-189, doi:https://doi.org/10.1006/viro.1998.9218 (1998).

60 Schmidt, S. *et al.* Allelic association of sequence variants in the herpes virus entry mediator-B gene (PVRL2) with the severity of multiple sclerosis. *Genes & Immunity* **7**, 384-392, doi:10.1038/sj.gene.6364311 (2006).

61 Kohio, H. P. & Adamson, A. L. Glycolytic control of vacuolar-type ATPase activity: A mechanism to regulate influenza viral infection. *Virology* **444**, 301-309, doi:https://doi.org/10.1016/j.virol.2013.06.026 (2013).

62 Yang, H. *et al.* Genetic Variants of the Receptor for Advanced Glycation End-products in Susceptibility to Type 2 Diabetes Mellitus in Primary Hypertensive Patients. *Scientific Reports* **7**, 17207, doi:10.1038/s41598-017-17068-9 (2017).

63 Manigrasso, M. B., Juranek, J., Ramasamy, R. & Schmidt, A. M. Unlocking the biology of RAGE in diabetic microvascular complications. *Trends in Endocrinology & Metabolism* **25**, 15-22, doi:10.1016/j.tem.2013.08.002 (2014).

64 Deane, R. *et al.* RAGE mediates amyloid-β peptide transport across the blood-brain barrier and accumulation in brain. *Nature Medicine* **9**, 907-913, doi:10.1038/nm890 (2003).

65 Miller, J. A., Woltjer, R. L., Goodenbour, J. M., Horvath, S. & Geschwind, D. H. Genes and pathways underlying regional and cell type changes in Alzheimer's disease. *Genome Med* **5**, 48-48, doi:10.1186/gm452 (2013).

66 Garske, K. M. *et al.* Reverse gene–environment interaction approach to identify variants influencing body-mass index in humans. *Nature Metabolism* **1**, 630-642, doi:10.1038/s42255-019-0071-6 (2019).

67 Agarwal, A. K. *et al.* Metabolic, Reproductive, and Neurologic Abnormalities in Agpat1-Null Mice. *Endocrinology* **158**, 3954-3973, doi:10.1210/en.2017-00511 (2017).

68 Sayas, C. L., Moreno-Flores, M. T., Avila, J. & Wandosell, F. The Neurite Retraction Induced by Lysophosphatidic Acid Increases Alzheimer's Disease-like Tau Phosphorylation. *Journal of Biological Chemistry* **274**, 37046-37052 (1999).

69 Nies, V. J. M. *et al.* Fibroblast Growth Factor Signaling in Metabolic Regulation. *Frontiers in Endocrinology* **6**, doi:10.3389/fendo.2015.00193 (2016).

70 Bodzęta, A., Kahms, M. & Klingauf, J. The Presynaptic v-ATPase Reversibly Disassembles and Thereby Modulates Exocytosis but Is Not Part of the Fusion Machinery. *Cell Reports* **20**, 1348-1359, doi:10.1016/j.celrep.2017.07.040 (2017).

71 Williamson, W. R. & Hiesinger, P. R. On the role of v-ATPase V0a1-dependent degradation in Alzheimer disease. *Commun Integr Biol* **3**, 604-607, doi:10.4161/cib.3.6.13364 (2010).

72 Peri, F. & Nüsslein-Volhard, C. Live Imaging of Neuronal Degradation by Microglia Reveals a Role for v0-ATPase a1 in Phagosomal Fusion In Vivo. *Cell* **133**, 916-927, doi:10.1016/j.cell.2008.04.037 (2008).

73 Dautry-Varsat, A. Receptor-mediated endocytosis: The intracellular journey of transferrin and its receptor. *Biochimie* **68**, 375-381, doi:https://doi.org/10.1016/S0300-9084(86)80004-9 (1986).

74 Faux, N. G. *et al.* An anemia of Alzheimer's disease. *Molecular Psychiatry* **19**, 1227-1234, doi:10.1038/mp.2013.178 (2014).

75 Fischer, P., Götz, M. E., Danielczyk, W., Gsell, W. & Riederer, P. Blood transferrin and ferritin in Alzheimer's disease. *Life Sciences* **60**, 2273-2278, doi:https://doi.org/10.1016/S0024-3205(97)00282-8 (1997).

76 Ward, R. J., Zucca, F. A., Duyn, J. H., Crichton, R. R. & Zecca, L. The role of iron in brain ageing and neurodegenerative disorders. *Lancet Neurol* **13**, 1045-1060, doi:10.1016/S1474-4422(14)70117-6 (2014).

77 Simcox, J. A. & McClain, D. A. Iron and diabetes risk. *Cell metabolism* **17**, 329-341, doi:10.1016/j.cmet.2013.02.007 (2013).

78 Kim, D. E. & Priefer, R. Therapeutic Potential of Direct Clearance of the Amyloid-β in Alzheimer's Disease. *Brain Sci* **10**, 93, doi:10.3390/brainsci10020093 (2020).

79 Loske, C. *et al.* Transition metal-mediated glycoxidation accelerates cross-linking of β-amyloid peptide. *European Journal of Biochemistry* **267**, 4171-4178, doi:10.1046/j.1432-1327.2000.01452.x (2000).

80 Kong, Y., Sharma, R. B., Nwosu, B. U. & Alonso, L. C. Islet biology, the CDKN2A/B locus and type 2 diabetes risk. *Diabetologia* **59**, 1579-1593, doi:10.1007/s00125-016-3967-7 (2016).

81 Emanuele, E. *et al.* Chromosome 9p21.3 genotype is associated with vascular dementia and Alzheimer's disease. *Neurobiology of Aging* **32**, 1231-1235, doi:https://doi.org/10.1016/j.neurobiolaging.2009.07.003 (2011).

82 Züchner, S. *et al.* Linkage and Association Study of Late-Onset Alzheimer Disease Families Linked to 9p21.3. *Annals of Human Genetics* **72**, 725-731, doi:10.1111/j.1469-1809.2008.00474.x (2008).

83 Lars Rödel, T. A., Gärtner, U. & Holzer, M. Expression of the cyclin-dependent kinase inhibitor p16 in Alzheimer's disease. *NeuroReport* **7** (1996).

84 McShea, A., Harris, P. L., Webster, K. R., Wahl, A. F. & Smith, M. A. Abnormal expression of the cell cycle regulators P16 and CDK4 in Alzheimer's disease. *Am J Pathol* **150**, 1933-1939 (1997).

85 Antonell, A. *et al.* Altered Blood Gene Expression of Tumor-Related Genes (PRKCB, BECN1, and CDKN2A) in Alzheimer's Disease. *Molecular Neurobiology* **53**, 5902-5911, doi:10.1007/s12035-015-9483-9 (2016).

86 Bonda, D. J. *et al.* Pathological implications of cell cycle re-entry in Alzheimer disease. *Expert Rev Mol Med* **12**, e19-e19, doi:10.1017/S146239941000150X (2010).

87 Kamrath, C., Hartmann, M. F. & Wudy, S. A. Androgen synthesis in patients with congenital adrenal hyperplasia due to 21-hydroxylase deficiency. *Horm Metab Res* **45**, 86-91, doi:10.1055/s-0032-1331751 (2013).

88 Lei, Y. & Renyuan, Z. Effects of Androgens on the Amyloid-β Protein in Alzheimer's Disease. *Endocrinology* **159**, 3885-3894, doi:10.1210/en.2018-00660 (2018).

89 Kiedrowicz, B. *et al.* Prevalence and Clinical Outcome of CYP21A2 Gene Mutations in Patients with Nonfunctional Adrenal Incidentalomas. *Horm Metab Res* **47**, 662-667, doi:10.1055/s-0035-1549911 (2015).

90 Kor, Y. *et al.* Phenotype heterogeneity of congenital adrenal hyperplasia due to genetic mosaicism and concomitant nephrogenic diabetes insipidus in a sibling. *BMC Med Genet* **19**, 115-115, doi:10.1186/s12881-018-0629-2 (2018).

91 Gambineri, A. & Pelusi, C. Sex hormones, obesity and type 2 diabetes: is there a link? *Endocr Connect* **8**, R1-R9, doi:10.1530/EC-18-0450 (2019).

92 Beulens, J. W. J. *et al.* Alcohol Consumption and Type 2 Diabetes. *Diabetes* **56**, 2388, doi:10.2337/db07-0181 (2007).

93 Borger, E. *et al.* Is amyloid binding alcohol dehydrogenase a drug target for treating Alzheimer's disease? *Current Alzheimer research* **10**, 21-29 (2013).

94 Bi, P. & Kuang, S. Notch signaling as a novel regulator of metabolism. *Trends Endocrinol Metab* **26**, 248-255, doi:10.1016/j.tem.2015.02.006 (2015).

95 Gupta, D., Kono, T. & Evans-Molina, C. The role of peroxisome proliferator-activated receptor γ in pancreatic β cell function and survival: therapeutic implications for the treatment of type 2 diabetes mellitus. *Diabetes Obes Metab* **12**, 1036-1047, doi:10.1111/j.1463-1326.2010.01299.x (2010).

96 Heneka, M. T., Reyes-Irisarri, E., Hüll, M. & Kummer, M. P. Impact and Therapeutic Potential of PPARs in Alzheimer's Disease. *Curr Neuropharmacol* **9**, 643-650, doi:10.2174/157015911798376325 (2011).

97 Krance, S. H. *et al.* The complement cascade in Alzheimer's disease: a systematic review and meta-analysis. *Molecular Psychiatry*, doi:10.1038/s41380-019-0536-8 (2019).

98 Shim, K., Begum, R., Yang, C. & Wang, H. Complement activation in obesity, insulin resistance, and type 2 diabetes mellitus. *World J Diabetes* **11**, 1-12, doi:10.4239/wjd.v11.i1.1 (2020).

99 Woo, H.-N., Park, J.-S., Gwon, A. R., Arumugam, T. V. & Jo, D.-G. Alzheimer's disease and Notch signaling. *Biochemical and Biophysical Research Communications* **390**, 1093-1097, doi:https://doi.org/10.1016/j.bbrc.2009.10.093 (2009).

100 Gallo, J.-M. *et al.* The Role of RNA and RNA Processing in Neurodegeneration. *The Journal of Neuroscience* **25**, 10372, doi:10.1523/JNEUROSCI.3453-05.2005 (2005).

101 Raj, T. *et al.* Integrative transcriptome analyses of the aging brain implicate altered splicing in Alzheimer's disease susceptibility. *Nature Genetics* **50**, 1584-1592, doi:10.1038/s41588-018-0238-1 (2018).

102 Mehta, M., Adem, A. & Sabbagh, M. New acetylcholinesterase inhibitors for Alzheimer's disease. *Int J Alzheimers Dis* **2012**, 728983-728983, doi:10.1155/2012/728983 (2012).

103 Scheuner, D. & Kaufman, R. J. The unfolded protein response: a pathway that links insulin demand with beta-cell failure and diabetes. *Endocr Rev* **29**, 317-333, doi:10.1210/er.2007-0039 (2008).

104 Norouzi, S., Adulcikas, J., Sohal, S. S. & Myers, S. Zinc transporters and insulin resistance: therapeutic implications for type 2 diabetes and metabolic disease. *J Biomed Sci* **24**, 87-87, doi:10.1186/s12929-017-0394-0 (2017).

105 Mizuno, D. & Kawahara, M. The molecular mechanisms of zinc neurotoxicity and the pathogenesis of vascular type senile dementia. *Int J Mol Sci* **14**, 22067-22081, doi:10.3390/ijms141122067 (2013).

106 Sensi, S. L., Granzotto, A., Siotto, M. & Squitti, R. Copper and Zinc Dysregulation in Alzheimer’s Disease. *Trends in Pharmacological Sciences* **39**, 1049-1063, doi:10.1016/j.tips.2018.10.001 (2018).

107 Wu, X. & Williams, K. J. Aquaporins-1 and -3 Play Novel, Distinct Roles in Normal Balanced Insulin Signaling. *Diabetes* **67**, 1781-P, doi:10.2337/db18-1781-P (2018).

108 Rainey-Smith, S. R. *et al.* Genetic variation in Aquaporin-4 moderates the relationship between sleep and brain Aβ-amyloid burden. *Translational Psychiatry* **8**, 47, doi:10.1038/s41398-018-0094-x (2018).

109 Smith, A. J., Duan, T. & Verkman, A. S. Aquaporin-4 reduces neuropathology in a mouse model of Alzheimer's disease by remodeling peri-plaque astrocyte structure. *Acta Neuropathologica Communications* **7**, 74, doi:10.1186/s40478-019-0728-0 (2019).

110 Robinson, D. *et al.* Androgen deprivation therapy for prostate cancer and risk of dementia. *BJU International* **124**, 87-92, doi:10.1111/bju.14666 (2019).

111 Manolio, T. A. *et al.* Finding the missing heritability of complex diseases. *Nature* **461**, 747-753, doi:10.1038/nature08494 (2009).

112 Yang, J. *et al.* Common SNPs explain a large proportion of the heritability for human height. *Nature Genetics* **42**, 565-569, doi:10.1038/ng.608 (2010).

113 Zuk, O., Hechter, E., Sunyaev, S. R. & Lander, E. S. The mystery of missing heritability: Genetic interactions create phantom heritability. *Proceedings of the National Academy of Sciences* **109**, 1193, doi:10.1073/pnas.1119675109 (2012).

114 Hekselman, I. & Yeger-Lotem, E. Mechanisms of tissue and cell-type specificity in heritable traits and diseases. *Nature Reviews Genetics* **21**, 137-150, doi:10.1038/s41576-019-0200-9 (2020).

115 Ishii, M. & Iadecola, C. Metabolic and Non-Cognitive Manifestations of Alzheimer's Disease: The Hypothalamus as Both Culprit and Target of Pathology. *Cell metabolism* **22**, 761-776, doi:10.1016/j.cmet.2015.08.016 (2015).

116 Lutsey, P. L., Steffen, L. M. & Stevens, J. Dietary intake and the development of the metabolic syndrome: the Atherosclerosis Risk in Communities study. *Circulation* **117**, 754-761, doi:10.1161/circulationaha.107.716159 (2008).

117 Cowie, C. C. *et al.* Full accounting of diabetes and pre-diabetes in the U.S. population in 1988-1994 and 2005-2006. *Diabetes Care* **32**, 287-294, doi:10.2337/dc08-1296 (2009).

118 Dhingra, R. *et al.* Soft drink consumption and risk of developing cardiometabolic risk factors and the metabolic syndrome in middle-aged adults in the community. *Circulation* **116**, 480-488, doi:10.1161/circulationaha.107.689935 (2007).

119 Stanhope, K. L., Schwarz, J. M. & Havel, P. J. Adverse metabolic effects of dietary fructose: results from the recent epidemiological, clinical, and mechanistic studies. *Curr Opin Lipidol* **24**, 198-206, doi:10.1097/MOL.0b013e3283613bca (2013).

120 Stanhope, K. L. *et al.* Consuming fructose-sweetened, not glucose-sweetened, beverages increases visceral adiposity and lipids and decreases insulin sensitivity in overweight/obese humans. *J Clin Invest* **119**, 1322-1334, doi:10.1172/jci37385 (2009).

121 Agrawal, R. & Gomez-Pinilla, F. 'Metabolic syndrome' in the brain: deficiency in omega-3 fatty acid exacerbates dysfunctions in insulin receptor signalling and cognition. *J Physiol* **590**, 2485-2499, doi:10.1113/jphysiol.2012.230078 (2012).

122 Ishimoto, T. *et al.* High-fat and high-sucrose (western) diet induces steatohepatitis that is dependent on fructokinase. *Hepatology* **58**, 1632-1643, doi:10.1002/hep.26594 (2013).

123 Lanaspa, M. A. *et al.* Endogenous fructose production and metabolism in the liver contributes to the development of metabolic syndrome. *Nat Commun* **4**, 2434, doi:10.1038/ncomms3434 (2013).

124 Macdonald, I. R. *et al.* Early Detection of Cerebral Glucose Uptake Changes in the 5XFAD Mouse. *Current Alzheimer Research* **11**, 450-460, doi:http://dx.doi.org/10.2174/1567205011666140505111354 (2014).

125 Ulland, T. K. *et al.* TREM2 Maintains Microglial Metabolic Fitness in Alzheimer's Disease. *Cell* **170**, 649-663.e613, doi:10.1016/j.cell.2017.07.023 (2017).

126 Meng, Q. *et al.* Systems Nutrigenomics Reveals Brain Gene Networks Linking Metabolic and Brain Disorders. *EBioMedicine* **7**, 157-166, doi:10.1016/j.ebiom.2016.04.008 (2016).

127 Gómez-Pinilla, F. Brain foods: the effects of nutrients on brain function. *Nat Rev Neurosci* **9**, 568-578, doi:10.1038/nrn2421 (2008).

128 Street, K. *et al.* Slingshot: cell lineage and pseudotime inference for single-cell transcriptomics. *BMC Genomics* **19**, 477-477, doi:10.1186/s12864-018-4772-0 (2018).

129 Jansen, I. E. *et al.* Genome-wide meta-analysis identifies new loci and functional pathways influencing Alzheimer's disease risk. *Nature Genetics* **51**, 404-413, doi:10.1038/s41588-018-0311-9 (2019).

130 Kunkle, B. W. *et al.* Genetic meta-analysis of diagnosed Alzheimer's disease identifies new risk loci and implicates Aβ, tau, immunity and lipid processing. *Nature genetics* **51**, 414-430, doi:10.1038/s41588-019-0358-2 (2019).

131 Subramanian, A. *et al.* A Next Generation Connectivity Map: L1000 Platform and the First 1,000,000 Profiles. *Cell* **171**, 1437-1452.e1417, doi:10.1016/j.cell.2017.10.049 (2017).

132 Zhou, Y. *et al.* Human and mouse single-nucleus transcriptomics reveal TREM2-dependent and TREM2-independent cellular responses in Alzheimer's disease. *Nature Medicine* **26**, 131-142, doi:10.1038/s41591-019-0695-9 (2020).

133 Rogers, J. T. *et al.* A role for amyloid precursor protein translation to restore iron homeostasis and ameliorate lead (Pb) neurotoxicity. *J Neurochem* **138**, 479-494, doi:10.1111/jnc.13671 (2016).

134 Michele, Z. *et al.* Complement C4A and C4B Gene Copy Number Study in Alzheimer's Disease Patients. *Current Alzheimer Research* **14**, 303-308, doi:http://dx.doi.org/10.2174/1567205013666161013091934 (2017).

135 Yang, C., Zhang, X., Gao, J., Wang, M. & Yang, Z. Arginine vasopressin ameliorates spatial learning impairments in chronic cerebral hypoperfusion via V1a receptor and autophagy signaling partially. *Translational Psychiatry* **7**, e1174-e1174, doi:10.1038/tp.2017.121 (2017).

136 Keren-Shaul, H. *et al.* A Unique Microglia Type Associated with Restricting Development of Alzheimer’s Disease. *Cell* **169**, 1276-1290.e1217, doi:10.1016/j.cell.2017.05.018 (2017).

137 He, W. *et al.* Reticulon family members modulate BACE1 activity and amyloid-β peptide generation. *Nature Medicine* **10**, 959-965, doi:10.1038/nm1088 (2004).

138 Zelikowsky, M. *et al.* The Neuropeptide Tac2 Controls a Distributed Brain State Induced by Chronic Social Isolation Stress. *Cell* **173**, 1265-1279.e1219, doi:https://doi.org/10.1016/j.cell.2018.03.037 (2018).

139 Fredericks, C. A. *et al.* Early affective changes and increased connectivity in preclinical Alzheimer's disease. *Alzheimers Dement (Amst)* **10**, 471-479, doi:10.1016/j.dadm.2018.06.002 (2018).

140 Mazurek, M. F., Beal, M. F., Bird, E. D. & Martin, J. B. Oxytocin in Alzheimer's disease. *Neurology* **37**, 1001, doi:10.1212/WNL.37.6.1001 (1987).

141 Mathys, H. *et al.* Single-cell transcriptomic analysis of Alzheimer's disease. *Nature* **570**, 332-337, doi:10.1038/s41586-019-1195-2 (2019).

142 Seddighi, S. *et al.* SPARCL1 Accelerates Symptom Onset in Alzheimer's Disease and Influences Brain Structure and Function During Aging. *J Alzheimers Dis* **61**, 401-414, doi:10.3233/JAD-170557 (2018).

143 Kurabayashi, N., Nguyen, M. D. & Sanada, K. The G protein-coupled receptor GPRC5B contributes to neurogenesis in the developing mouse neocortex. *Development* **140**, 4335, doi:10.1242/dev.099754 (2013).

144 Soni, A., Amisten, S., Rorsman, P. & Salehi, A. GPRC5B a putative glutamate-receptor candidate is negative modulator of insulin secretion. *Biochemical and Biophysical Research Communications* **441**, 643-648, doi:https://doi.org/10.1016/j.bbrc.2013.10.099 (2013).

145 Block, M. L., Zecca, L. & Hong, J. S. Microglia-mediated neurotoxicity: uncovering the molecular mechanisms. *Nat Rev Neurosci* **8**, 57-69, doi:10.1038/nrn2038 (2007).

146 Lai, A. Y. & McLaurin, J. Clearance of amyloid-β peptides by microglia and macrophages: the issue of what, when and where. *Future Neurol* **7**, 165-176, doi:10.2217/fnl.12.6 (2012).

147 Emilsson, V. *et al.* Genetics of gene expression and its effect on disease. *Nature* **452**, 423-428, doi:10.1038/nature06758 (2008).

148 Derry, J. M. J. *et al.* Identification of genes and networks driving cardiovascular and metabolic phenotypes in a mouse F2 intercross. *PLoS One* **5**, e14319-e14319, doi:10.1371/journal.pone.0014319 (2010).

149 Wang Susanna, S. *et al.* Identification of Pathways for Atherosclerosis in Mice. *Circulation Research* **101**, e11-e30, doi:10.1161/CIRCRESAHA.107.152975 (2007).

150 Schadt, E. E. *et al.* Mapping the Genetic Architecture of Gene Expression in Human Liver. *PLOS Biology* **6**, e107, doi:10.1371/journal.pbio.0060107 (2008).

151 Tu, Z. *et al.* Integrative Analysis of a Cross-Loci Regulation Network Identifies App as a Gene Regulating Insulin Secretion from Pancreatic Islets. *PLOS Genetics* **8**, e1003107, doi:10.1371/journal.pgen.1003107 (2012).

152 Yang, X. *et al.* Tissue-specific expression and regulation of sexually dimorphic genes in mice. *Genome Res* **16**, 995-1004, doi:10.1101/gr.5217506 (2006).

153 Kang, H. J. *et al.* Spatio-temporal transcriptome of the human brain. *Nature* **478**, 483-489, doi:10.1038/nature10523 (2011).